The endosomal trafficking factors CORVET and ESCRT suppress plasma membrane residence of the renal outer medullary potassium channel (ROMK)

Received for publication, September 20, 2017, and in revised form, January 2, 2018 Published, Papers in Press, January 8, 2018, DOI 10.1074/jbc.M117.819086

Timothy D. Mackie[‡], Bo-Young Kim[§], Arohan R. Subramanya[¶‖], Daniel J. Bain[**], Allyson F. O'Donnell[‡‡], Paul A. Welling[§], and Jeffrey L. Brodsky[‡1]

From the Departments of [‡]Biological Sciences and [**]Geology and Environmental Science, University of Pittsburgh, Pittsburgh, Pennsylvania 15260, the [§]Department of Physiology, University of Maryland at Baltimore, Baltimore, Maryland 21201, the [¶]Departments of Medicine and Cell Biology, University of Pittsburgh, Pittsburgh, Pennsylvania 15261, the [‖]Medicine and Research Services, Veterans Affairs Pittsburgh Healthcare System, Pittsburgh, Pennsylvania 15240, and the [‡‡]Department of Biological Sciences, Duquesne University, Pittsburgh, Pennsylvania 15282

Edited by Peter Cresswell

Protein trafficking can act as the primary regulatory mechanism for ion channels with high open probabilities, such as the renal outer medullary (ROMK) channel. ROMK, also known as Kir1.1 (KCNJ1), is the major route for potassium secretion into the pro-urine and plays an indispensable role in regulating serum potassium and urinary concentrations. However, the cellular machinery that regulates ROMK trafficking has not been fully defined. To identify regulators of the cell-surface population of ROMK, we expressed a pH-insensitive version of the channel in the budding yeast *Saccharomyces cerevisiae*. We determined that ROMK primarily resides in the endoplasmic reticulum (ER), as it does in mammalian cells, and is subject to ER-associated degradation (ERAD). However, sufficient ROMK levels on the plasma membrane rescued growth on low-potassium medium of yeast cells lacking endogenous potassium channels. Next, we aimed to identify the biological pathways most important for ROMK regulation. Therefore, we used a synthetic genetic array to identify non-essential genes that reduce the plasma membrane pool of ROMK in potassium-sensitive yeast cells. Genes identified in this screen included several members of the endosomal complexes required for transport (ESCRT) and the class-C core vacuole/endosome tethering (CORVET) complexes. Mass spectroscopy analysis confirmed that yeast cells lacking an ESCRT component accumulate higher potassium concentrations. Moreover, silencing of ESCRT and CORVET components increased ROMK levels at the plasma membrane in HEK293 cells. Our results indicate that components of the post-endocytic pathway influence the cell-surface density of ROMK and establish that components in this pathway modulate channel activity.

This work was supported by National Institutes of Health Grants GM75061 and DK79307 (University of Pittsburgh George O'Brien Kidney Research Center) (to J. L. B.), R01DK098145 (to A. R. S.), and DK054231 (to P. A. W.) and by National Science Foundation MCB CAREER Grant 1553143 (to A. F. O.). The authors declare that they have no conflicts of interest with the contents of this article. The content is solely the responsibility of the authors and does not necessarily represent the official views of the National Institutes of Health.

This article contains Figs. S1–S8 and Tables S1–S4.

[1] To whom correspondence should be addressed: A320 Langley Hall, 4249 Fifth Ave., Pittsburgh, PA 15260. Tel.: 412-624-4831; E-mail: jbrodsky@pitt.edu.

Protein quality control allows cells in all organisms to survive proteotoxic stresses and to fine-tune their proteome in response to environmental changes (1). Significant recent work has elucidated in great detail how protein quality control pathways operate in the cytoplasm and in the endoplasmic reticulum (ER)[2] (2–4). Common to both pathways is the delivery of substrates to the cytoplasmic proteasome, which selectively degrades ubiquitinated and misfolded protein substrates (5). In addition, proteins that reside in the ER or in the ER membrane must be removed from this compartment and delivered to the proteasome. The selection, delivery, and degradation of misfolded proteins in this compartment proceeds through the ER-associated degradation (ERAD) pathway. Quality control "decisions" that operate at later steps in the secretory pathway, such as in the Golgi apparatus, the endosome, and the plasma membrane, have also been identified in eukaryotic cells (6–8). However, the relative influence of each system on specific client proteins is rarely investigated.

One critical class of proteins that transit the secretory pathway and might be subject to more than one quality control checkpoint are ion channels. Even under ideal circumstances, ion channels may possess unfavorable folding kinetics or are thermodynamically unstable because of dynamic structural transitions and/or because charged and hydrophilic residues reside within their transmembrane domains (9). Long-range interactions between channel domains or even between channel subunits further compromise folding efficiency (10). Perhaps not surprisingly, genetic mutations that exacerbate protein misfolding result in degradation by cellular protein quality control pathways, including ERAD and the late secretory quality control pathways, noted above (11). For example, the cystic fibrosis transmembrane conductance regulator (CFTR)

[2] The abbreviations used are: ER, endoplasmic reticulum; ERAD, ER-associated degradation; ROMK, renal outer medullary potassium; ESCRT, endosomal complexes required for transport; CORVET, class-C core vacuole/endosome tethering; CFTR, cystic fibrosis transmembrane conductance regulator; PMSF, phenylmethylsulfonyl fluoride; DPBS, Dulbecco's phosphate-buffered saline; ICP-MS, inductively coupled plasma-mass spectrometry; SGA, synthetic genetic array; GO, gene ontology; MVB, multivesicular body; Vn, Venus-tagged; RFP, red fluorescent protein.

requires ~30 min from the onset of translation to reach its native conformation, during which ~70% of the wildtype channel is recognized as being misfolded and is targeted for ERAD (12, 13). The predominant cystic fibrosis-causing allele, ΔF508, interferes with the assembly of a soluble domain that engages a transmembrane domain-containing segment (14, 15), so essentially all of the mutant protein is degraded by ERAD. Moreover, even if the mutant is released to the plasma membrane, either through the application of chemical chaperones or by low temperature incubation, it is more rapidly endocytosed than the wildtype protein and destroyed in the lysosome via plasma membrane quality control (16). Furthermore, ΔF508-containing aggregates have been detected in cells, which may be selected for degradation in the lysosome via the autophagic pathway (17). Studies of multimeric ion channels, such as the voltage-gated potassium channel human *Ether-à-go-go* Related Gene (hERG), have found that subunit assembly can also present an energetic barrier during ion channel maturation (18). In addition, hERG mutants associated with long-Q-T syndrome are degraded by ERAD in a chaperone- and proteasome-dependent manner (19–21). Together, these data emphasize the inefficient nature of ion channel biogenesis and indicate that disease-causing mutations can interfere with protein folding in the secretory pathway.

In addition to CFTR and hERG, the impact of cellular quality control mechanisms in the regulation of other disease-associated ion channels has also been investigated (11, 20, 22–29). However, the rules that govern the quality control of diverse ion channels remain poorly defined. We propose that a continued investigation into the mechanisms underlying the biogenesis and degradation of ion channels will help uncover these rules and define how associated "channelopathies" might be treated.

To this end, we initiated studies on the homo-tetrameric renal outer medullary potassium (ROMK) channel, also known as Kir1.1. ROMK is the primary potassium efflux channel in the thick ascending limb and distal nephron (30) and is expressed as two major isoforms with divergent physiological roles. ROMK2 is primarily expressed in the thick ascending limb of the loop of Henle and is responsible for potassium cycling coupled to sodium and chloride reabsorption through the sodium potassium chloride cotransporter, NKCC2. In contrast, bulk potassium secretion via ROMK1 occurs in the late distal convoluted tubule, connecting tubule, and cortical collecting duct, and ROMK1 expression is increased in response to dietary potassium intake (31, 32). Under physiological conditions, both ROMK isoforms have a high open probability (P_o) of ~0.9 (33, 34), so channel expression must be tightly regulated due to its vital role in regulating serum potassium levels. Indeed, ROMK function is thought to be regulated primarily through the homeostatic control of protein trafficking (35–38). In addition, mutations that deplete ROMK from the plasma membrane cause an autosomal recessive salt-wasting disorder known as type II Bartter syndrome (39). Interestingly, individuals heterozygous for a type II Bartter mutant allele exhibit resistance to hypertension, most likely because of decreased NKCC2-mediated reabsorption of sodium (40). Of the >50 identified Bartter syndrome-associated mutations in ROMK, many appear to affect ROMK trafficking or post-translational modification when ectopically expressed in *Xenopus laevis* oocytes (41). To date, therapies for Bartter syndrome are not curative, and patients require lifelong multidrug treatments and potassium supplementation. Thus, a deeper understanding of the trafficking and degradative machineries that shepherd ROMK to and from the plasma membrane is necessary to devise effective treatments for type II Bartter syndrome.

In this study, we used the budding yeast *Saccharomyces cerevisiae* to define the relative contributions of protein trafficking and two distinct quality control pathways on ROMK stability and plasma membrane residence. As deleting the genes encoding two plasma membrane potassium channels, *TRK1* and *TRK2*, renders yeast inviable on low-potassium media (42), an ectopically expressed potassium channel, such as ROMK, can rescue this phenotype, assuming that it is able to fold, assemble, and traffic to the plasma membrane (Fig. 1*A*). Previous studies by our group and other groups have exploited this technique for structure–function and genetic interaction studies of several human potassium channels (27, 43–47). Here, we report on a new yeast screen to monitor growth on low potassium as a readout for genes that increase ROMK function at the plasma membrane. By screening the yeast non-essential deletion collection (49), we identified two complexes with established roles in post-endocytic trafficking that regulate the plasma membrane levels of ROMK: the endosomal complexes required for trafficking (ESCRT) and the class-C core vacuole/endosome tethering (CORVET) complex. We then confirmed the biological relevance of these complexes by silencing select ESCRT and CORVET homologs in human cells. These data provide the first genome-wide analysis of factors that control ROMK biogenesis, and our work led to the identification of components that, in principle, can be therapeutically modulated to treat disorders associated with ROMK function.

Results

Identification of a ROMK variant suitable for high-throughput genetic analysis

We recently reported that two targeted mutations in ROMK are necessary to ensure a screenable phenotype in *trk1*Δ*trk2*Δ yeast on low-potassium medium (50). These mutations prevent the gating of ROMK by low pH, which is common in the yeast cytosol, and replace Ser with a phospho-mimetic amino acid, Asp, at position 44, which favors channel egress from the ER to the Golgi apparatus (51, 52). This form of ROMK was then used to show that type II Bartter syndrome mutations fail to rescue the growth of *trk1*Δ*trk2*Δ yeast on low-potassium medium (50). In addition, our group previously performed a synthetic genetic array (SGA) in *trk1*Δ*trk2*Δ yeast on low-potassium medium to identify genes that regulate the plasma membrane residence of another human potassium channel, Kir2.1. This study uncovered a component of complex I of the ESCRT complex (ESCRT-I), Vps23, as a negative regulator of Kir2.1 in both yeast and human cells (27). Because ROMK and Kir2.1 are 42% identical and are members of the inward-rectifying potassium channel family, Kir2.1 expressed in *trk1*Δ*trk2*Δ*vps23*Δ yeast was used as a positive control. As reported previously, *trk1*Δ*trk2*Δ*vps23*Δ yeast expressing Kir2.1 are able to grow on

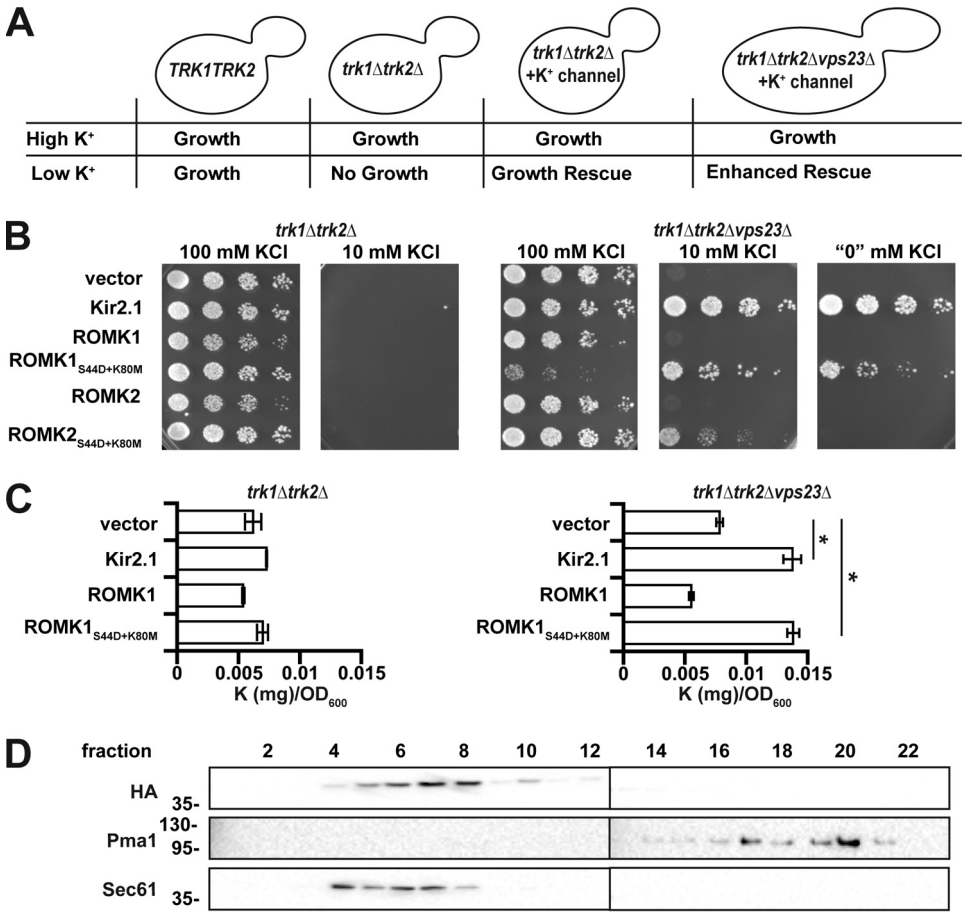

Figure 1. ROMK1$_{S44D+K80M}$ rescues growth of *trk1Δtrk2Δ* yeast on low potassium and increases potassium uptake. *A,* representation of a yeast-based assay for potassium channel function. *B,* yeast strains with the indicated genotypes transformed with an empty expression vector control or vectors engineered to express Kir2.1, wildtype ROMK1, ROMK1$_{S44D+K80M}$, ROMK2, or ROMK2$_{S44D+K80M}$ were serially diluted onto medium supplemented with the indicated amounts of KCl. *C,* intracellular potassium levels, as measured by ICP-MS, were assessed using equivalent amounts of yeast containing an empty vector or expressing Kir2.1, wildtype ROMK1, or ROMK1$_{S44D+K80M}$. Cells were cultured for 8 h in liquid media containing either 100 or 10 mM KCl. Data show the means of three biological replicates. *Error bars* show standard deviations, *, $p < 0.05$ (Student's *t* test). *D,* Western blottings of sucrose gradient fractions showing migration of HA-tagged ROMK1$_{S44D+K80M}$ containing microsomes in wildtype yeast. Pma1 marks the plasma membrane-derived fractions, and Sec61 marks ER-derived fractions.

low (10 mM)-potassium medium, whereas *trk1Δtrk2Δ* yeast transformed with an empty expression vector are not (Fig. 1*B*).

We next tested the two alternatively spliced isoforms in the kidney, ROMK1 and ROMK2, which are identical except for a 19-amino acid residue N-terminal extension in ROMK1. To date, no biophysical differences between the channels have been identified, although they have divergent physiological roles (35). Curiously, ROMK2$_{S44D+K80M}$ failed to rescue the growth of *trk1Δtrk2Δvps23Δ* yeast on low-potassium media as effectively as ROMK1$_{S44D+K80M}$ (Fig. 1*B*), despite somewhat higher steady-state expression levels of ROMK2$_{S44D+K80M}$ compared with ROMK1$_{S44D+K80M}$ (Fig. S1). Notably, the degree of rescue mediated by ROMK1$_{S44D+K80M}$ was similar to that of Kir2.1, which was used in our previous screen. Hence, ROMK1$_{S44D+K80M}$ was used for the remainder of this study. Furthermore, we predicted that the ROMK1$_{S44D+K80M}$ protein could be used to conduct an SGA analysis, which could provide for the first time a whole genomic profile of the factors that negatively regulate ROMK trafficking.

To confirm that Kir2.1 and ROMK1$_{S44D+K80M}$ directly increase the concentration of intracellular potassium in *trk1Δtrk2Δ* yeast, we prepared extracts from yeast cells expressing these proteins, as well as from those containing a vector control, and subjected the extracts to inductively coupled plasma-mass spectrometry (ICP-MS). This method allows for precise measurement of the metallic elemental composition of a biological sample. We first noted that the level of intracellular potassium in *trk1Δtrk2Δ* yeast expressing ROMK1$_{S44D+K80M}$ was not statistically different from the vector control after ~8 h of culture in medium containing 10 mM potassium (Fig. 1*C*, *left graph*). These data are consistent with the inability of this strain to grow better than the control in the same medium (Fig. 1*B*). However, both Kir2.1 and ROMK1$_{S44D+K80M}$ expression increased intracellular potassium more than 2-fold compared with the control in *trk1Δtrk2Δvps23Δ* cells (Fig. 1*C*, *right graph*), consistent with Vps23 acting as a negative regulator of ROMK.

Prior studies established that *trk1Δtrk2Δ* yeast are sensitive to the toxic cations hygromycin B (an aminoglycoside antibiotic), spermine, and tetramethylammonium (53). This phenotype arises from increased cellular uptake of the toxins in *trk1Δtrk2Δ* yeast because the membrane is hyperpolarized when potassium entry is limited. Therefore, we examined

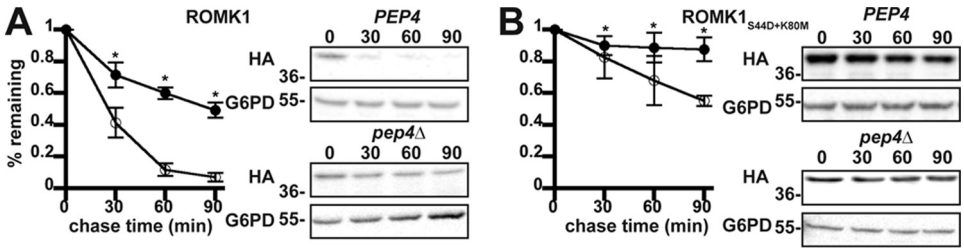

Figure 2. ROMK1 and ROMK1$_{S44D+K80M}$ are degraded to varying degrees by the vacuole in yeast. Yeast cultures expressing HA-tagged versions of either ROMK1 (*A*) or ROMK1$_{S44D+K80M}$ (*B*) grown to mid-logarithmic phase were dosed with cycloheximide, and aliquots were withdrawn at 0, 30, 60, and 90 min. A yeast strain lacking the master vacuolar protease (*pep4*Δ, *filled circles*) or an isogenic wildtype (*PEP4*, *open circles*) expressing the proteins were shifted from room temperature to 37 °C 30 min before addition of cycloheximide. ROMK expression was assessed by Western blotting, and data were normalized to the initial time point. Representative blots are shown, and all blots were stripped and reprobed for glucose-6-phosphate dehydrogenase (*G6PD*) as a loading control. Data represent the means of six independent experiments from two independent yeast transformations. *Error bars* show standard errors of the mean; * indicates a significant ($p < 0.05$) difference as assessed by Student's *t* test.

growth on medium containing hygromycin B. Consistent with data in Fig. 1*B*, Kir2.1 or ROMK1$_{S44D+K80M}$ expression enhanced *trk1*Δ*trk2*Δ*vps23*Δ yeast growth on medium supplemented with hygromycin B (Fig. S2). Together, these results indicate that ROMK1$_{S44D+K80M}$ functions as a potassium transporter in yeast, allowing for sufficient import of this cation to support growth on low-potassium medium.

When examined under steady-state conditions in mammalian cells, ROMK primarily resides in the ER (35, 41). Similarly, we found that the majority of ROMK1$_{S44D+K80M}$ comigrated with the ER-resident protein Sec61 when lysates from a wildtype yeast strain isogenic to *trk1*Δ*trk2*Δ and its derivatives (BY4742) were subjected to subcellular fractionation by sucrose gradient sedimentation analysis (Fig. 1*D*). ROMK appeared to be absent in the Pma1-containing plasma membrane fractions. Based on the clear increase in intracellular potassium and the phenotypic data presented above, these results suggest that ROMK1$_{S44D+K80M}$ growth rescue on low-potassium medium requires only small amounts of protein at the plasma membrane that are undetectable using this approach (also see below). This conclusion is consistent with our previous data, indicating that very low levels of Kir2.1 plasma membrane residence are sufficient for growth rescue under these steady-state conditions (27, 50).

ROMK1$_{S44D+K80M}$ is primarily degraded by the vacuole and not by ERAD in yeast

ERAD is one of the first lines of defense against the accumulation of misfolded proteins in the secretory pathway. We recently reported that ROMK1$_{S44D+K80M}$ is more stable than wildtype ROMK1 in yeast and *in vitro* (50), but the relative contribution of ERAD *versus* post-ER quality control mechanisms was not investigated. Moreover, neither ROMK1 nor ROMK1$_{S44D+K80M}$ was completely stable when the proteasome was inhibited with MG132. These data suggest that a sub-population of ROMK is degraded in the vacuole, which serves as the degradative compartment for post-ER quality control in yeast (54) To determine whether the vacuole contributes directly to ROMK degradation, both wildtype ROMK1 and ROMK1$_{S44D+K80M}$ were expressed in a yeast strain lacking Pep4, which activates proteases in the vacuole by cleaving their immature forms (55), as well as in an isogenic wildtype strain. We then analyzed their relative degradation profiles in a cycloheximide chase assay. As shown in Fig. 2, both ROMK variants were significantly stabilized in *pep4*Δ yeast. However, although ROMK1 was only partially stabilized (Fig. 2*A*), consistent with targeting to the ERAD pathway, ROMK1$_{S44D+K80M}$ was almost completely stable within the 90-min time scale of the chase (Fig. 2*B*). These data also emphasized the overall heightened stability of the ROMK1$_{S44D+K80M}$ protein as compared with wildtype ROMK1 (50).

We next examined the relative efficiencies with which wildtype ROMK1 and the ROMK1$_{S44D+K80M}$ isoform are degraded by ERAD. During ERAD, misfolded protein substrates are recognized by molecular chaperones such as Hsp70 and ubiquitinated by E3 ubiquitin ligases that are ER-associated (2, 4). After the acquisition of a polyubiquitin tag, the ERAD substrate is retrotranslocated from the ER in an ATP-dependent process that utilizes the AAA-ATPase, Cdc48 (in yeast), or p97 (in mammals). We found that wildtype ROMK1 behaves like a canonical yeast ERAD substrate as it was significantly stabilized when Cdc48 was inactivated, when the genes encoding two ER-localized E3 ubiquitin ligases in yeast, Hrd1 and Doa10, were deleted, or when the cytosolic Hsp70 Ssa1 was disabled (Fig. 3, *A, C,* and *E*). However, ROMK1$_{S44D+K80M}$ was consistently more stable, and the relative amount of degradation was affected less or not at all by ablation of these ERAD components (Fig. 3, *B, D,* and *F*). We propose that the degradation of wildtype ROMK1 is dominated by ERAD, whereas the degradation of ROMK1$_{S44D+K80M}$ is dominated by post-ER quality control. Therefore, ROMK1$_{S44D+K80M}$ represents a novel "tool" with which to decipher how the post-ER quality control machinery regulates channel levels.

Yeast SGA for ROMK1 effectors implicates late secretory pathway protein degradation

Because ROMK1$_{S44D+K80M}$ rescues potassium sensitivity in *trk1*Δ*trk2*Δ*vps23*Δ yeast and appears to do so by increasing intracellular potassium (Fig. 1, *B* and *C*) (50), we conducted a whole-genome screen for other factors that negatively regulate ROMK residence and activity at the plasma membrane. To this end, ROMK1$_{S44D+K80M}$-expressing *trk1*Δ*trk2*Δ yeast were mated with the non-essential yeast deletion collection, and arrays of triple mutant progeny (*i.e.* those that were deleted for *TRK1*, *TRK2*, and a non-essential gene; see under "Experimental procedures") were generated (Fig. 4*A*). Potential negative effectors were identified by comparing growth on high (100 mM) *versus* low ("0" mM) potassium medium, in which the only

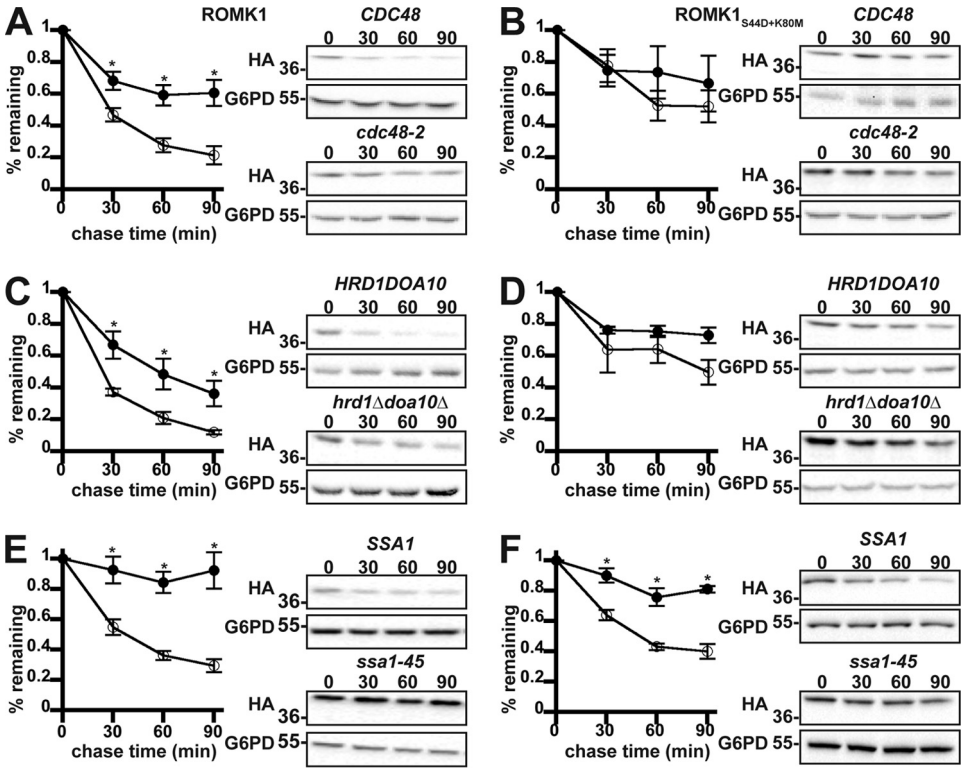

Figure 3. ROMK1 is degraded by the ERAD pathway to a greater extent than ROMK1$_{S44D+K80M}$ in yeast. Yeast cultures expressing HA-tagged versions of either ROMK1 (*A, C,* and *E*) or ROMK1$_{S44D+K80M}$ (*B, D,* and *F*) grown to mid-logarithmic phase were dosed with cycloheximide, and aliquots were withdrawn at 0, 30, 60, and 90 min. Yeast strains containing either a temperature-sensitive mutation in the gene encoding Cdc48 (*cdc48-2*, *filled circles*) or lacking the mutant allele (*CDC48*, *open circles*) expressing wildtype ROMK1 (*A*) or ROMK1$_{S44D+K80M}$ (*B*) were shifted from room temperature to 39 °C for 60 min before addition of cycloheximide. A yeast strain lacking the ER-resident E3 ubiquitin ligases (*hrd1Δdoa10Δ*, *filled circles*) or an isogenic wildtype strain (*HRD1DOA10*, *open circles*) expressing wildtype ROMK1 (*C*) or ROMK1$_{S44D+K80M}$ (*D*) were shifted from room temperature to 37 °C 30 min before addition of cycloheximide. Yeast strains lacking four cytosolic isoforms of Hsp70 (Ssa1, Ssa2, Ssa3, and Ssa4) and containing either a temperature-sensitive mutation of Ssa1 (*ssa1-45*, *filled circles*) or an isogenic wildtype allele (*SSA1*, *open circles*) and expressing wildtype ROMK1 (*E*) or ROMK1$_{S44D+K80M}$ (*F*) were shifted from room temperature to 37 °C 30 min before addition of cycloheximide. For all experiments, ROMK expression was assessed by Western blotting and normalized to the initial time point. Representative images are shown, and all blots were stripped and reprobed for glucose-6-phosphate dehydrogenase (*G6PD*) as a loading control. Data represent the means of six independent experiments from two independent yeast transformations. *Error bars* show standard errors of the mean, and *indicates a significant ($p < 0.05$) difference as assessed by Student's *t* test.

available potassium derives from trace amounts in the media components (42). The initial screen revealed 40 very strong hits (z-score >3), 228 strong hits (z-score >2), and 519 weak hits (z-score >1) from the nearly 5,000 strains screened (Table S1). The confirmed negative regulator of ROMK, *VPS23* (see above), was among the very strong hits from the screen. We then re-arrayed select parental strains representing the 228 strong and very strong hits into fresh 96-well plates and performed the screen a second time to eliminate false positives. For the purposes of this study, we also eliminated from consideration genes known to sensitize yeast to toxic cations, such as members of the remodels the structure of chromatin (RSC) complex (53). GO-term analysis of the 40 confirmed strongest hits indicated a positive ($p < 0.05$) enrichment for the terms "endosomal transport," "late endosome to vacuole transport," and "vacuolar transport," each of which are components of the late secretory trafficking and quality control machineries (Fig. 4*B*). Other genes associated with these pathways were also represented among the strong (z-score >2) and weak (z-score >1) hits.

Next, to further increase our confidence in select hits, we reconstructed several of the triple mutant strains *de novo* by manually mating *trk1Δtrk2Δ* with the appropriate strain from the deletion collection, inducing sporulation, micro-dissecting the resultant tetrads, and selecting triple knockout progeny (Fig. 4*C*, *underlined*). This step was necessary to correct for false positives from the original list of screen hits and to build a trustworthy set of strains for subsequent experiments. Select strains that were absent from the original screen were also included in this curated list as they are well-characterized components of the endosome-to-vacuole sorting pathway and genetically interact with the isolated hits (Fig. 4*C*). The parental strains from the deletion collection corresponding to those in this curated list were confirmed by PCR (see "Experimental procedures"). The reconstructed strains were then transformed with a vector control or the Kir2.1, ROMK1, or ROMK1$_{S44D+K80M}$ expression vectors. Transformants were serially diluted onto a range of potassium-supplemented media, and yeast expressing ROMK1$_{S44D+K80M}$ that grew better on low ("0" or 10 mM) concentrations of potassium relative to the vector control were considered to be verified negative regulators of ROMK (Fig. 5 and Fig. S3). Importantly, the relative amounts of Kir2.1, ROMK1, and ROMK1$_{S44D+K80M}$ in these strains did not reflect the degree to which growth was rescued (Fig. S4), suggesting that the primary effect of the mutants was

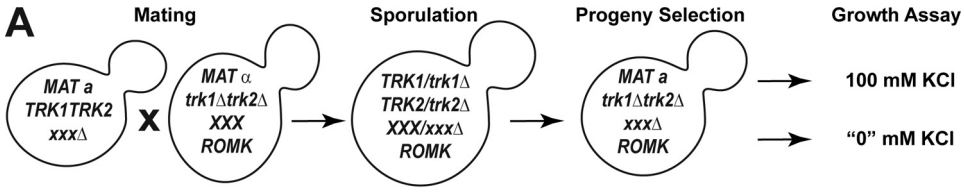

B

GO Term	Genes
ATP-dependent chromatin remodeling	*SWC5, SWR1, RSC1, RSC2, BDF1, NPL6*
Nucleosome organization	*SWC5, SWR1, RSC1, RSC2, BDF1, NPL6*
Chromatin remodeling	*SWC5, SWR1, RSC1, RSC2, BDF1, NPL6*
Histone exchange	*SWC5,SWR1,BDF2*
DNA-templated transcription, elongation	*RSC1, RSC2, NPL6, NPL3, RPA49*
Protein-DNA complex subunit organization	*SWC5, SWR1, RSC1, RSC2, BDF1, NPL6*
Chromatin disassembly	*RSC1, RSC2, NPL6*
Protein-DNA complex disassembly	*RSC1, RSC2, NPL6*
Endosomal transport	*VPS8, VPS23, YPT7, VPS20, VPS21*
Late endosome to vacuole transport	*VPS8, VPS23, VPS20, VPS21*
Vacuolar transport	*VPS8, VPS23, VPS64, YPT7, VPS20, VPS21*

C

Family	Function	Genes
CORVET	Tether Early Endosomes	*VPS3*, ***VPS8***, *VPS18*, *VAM6*, *VPS11*, *VPS16*
HOPS	Tether Late Endosomes	*VPS39*, *VPS41*, *VPS18*, *VAM6*, *VPS11*, *VPS16*
ESCRT-0	Bind Ubiquitinated Cargo	***VPS27***, *HSE1*
ESCRT-I	Recruit Cargo to ILVs	***VPS23***,*VPS28, VPS37, MVB12*
ESCRT-II	Recruit Cargo to ILVs	*VPS22, VPS25,* ***VPS36***
ESCRT-III	Invaginate ILVs	*VPS2,* ***VPS20***, *VPS24, SNF7*
Vps4C	Sever ILVs	***VPS4***, *VPS60, VTA1*
Retromer	Return Cargo to Golgi	***VPS5***, *VPS17, VPS26, VPS29, VPS35*
Rsp5 Adaptors	Promote Ubiquitination	***SSH4***, *BSD2, EAR1*
SNAREs	Fuse Membranes	***TVP15***, ***TVP23***, *TGL6, VAM7, PEP12,* ***GOS1***
Rab GTPases and cofactors	Identify Endosomal Sub-Populations	***VPS21***, ***YPT7***, *YPT10,* ***MSB3***, *MSB4, VPS9,* ***BTS2***

Figure 4. Endosomal sorting genes are key negative regulators of ROMK at the cell surface. *A,* representation of the synthetic genetic array screen. *B,* GO term analysis of very strong hits (*z*-score >3) isolated from initial screen listed in increasing order of *p* values from the most significant (<0.001) to the least significant (<0.05). *C,* endosomal transport genes considered for further investigation in this study. Genes are arranged by functional classification. Genes in *boldface* were identified in the screen, whereas those in *normal type* were selected as known interactors with identified genes. *Underlined genes* were selected for *de novo* strain reconstruction.

on protein residence at the plasma membrane and not only on changes in global protein levels.

To bolster our confidence that the observed rescue of growth on low-potassium medium correlates with an increase in ROMK plasma membrane residence, we next conducted sucrose gradient analysis on fractionated membranes derived from *end3*Δ potassium-sensitive yeast and an isogenic wildtype strain. In the *end3*Δ background, which is endocytosis-deficient, a small amount of $ROMK1_{S44D+K80M}$ appears to comigrate with the plasma membrane marker Pma1 when gels analyzing fractions from the gradient were overexposed (Fig. S5, *A* and *B,* "long exposure"). A signal corresponding to the plasma membrane was not evident when lysates from wildtype cells were examined (Fig. S5*A*). Thus, even though the amount of the protein at the plasma membrane is quite low, $ROMK1_{S44D+K80M}$ promotes robust rescue of potassium-sensitive growth in *end3*Δ yeast (Fig. S5, *C* and *D*). This phenomenon most likely arises from the high P_o reported for ROMK (33, 34).

Vps8, a subunit of the CORVET complex, was identified as one of the strongest hits from the initial screen (Figs. 4 and 5). The CORVET complex is a heterohexamer involved in tethering vesicles containing Vps21, which is the yeast Rab5 homolog, prior to early endosome biogenesis (56). CORVET shares four out of six subunits with the HOPS complex, which performs a similar role as CORVET. However, HOPS instead functions with vesicles containing Ypt7, which is the yeast Rab7 homolog, to promote fusion of multivesicular bodies (MVBs) with the vacuole (57, 58). Components of both complexes are conserved from yeast to man (59–61). Therefore, to determine whether CORVET and/or HOPS functioned as novel, negative regulators of ROMK, both unique and shared CORVET and HOPS knockout strains were generated in the *trk1*Δ*trk2*Δ background. We discovered that only deletion of the CORVET-specific subunits Vps3 and Vps8 improved the growth of *trk1*Δ*trk2*Δ yeast expressing $ROMK1_{S44D+K80M}$ (Fig. 5, *B* and *C*). In contrast, deletion of the HOPS-specific subunits Vps39 and Vps41 and shared subunits Vps11, Vps16, Vps18, and Vps33 had no or little effect on growth (data not shown). A model to explain these data is provided under the "Discussion."

Several other strong hits, as measured by the degree of growth rescue on low potassium, included strains lacking the ubiquitin-binding subunits of the four ESCRT complexes: Vps27 (ESCRT-0), Vps23 (ESCRT-I), Vps36 (ESCRT-II), and Vps20 (ESCRT-III) (Fig. 5, *D–H*). The ESCRTs act sequentially to recruit ubiquitinated endocytic and Golgi-derived cargo into the MVB degradation pathway (62). ESCRT targeting is primarily mediated by the cytoplasmic E3 ubiquitin ligase Rsp5 in

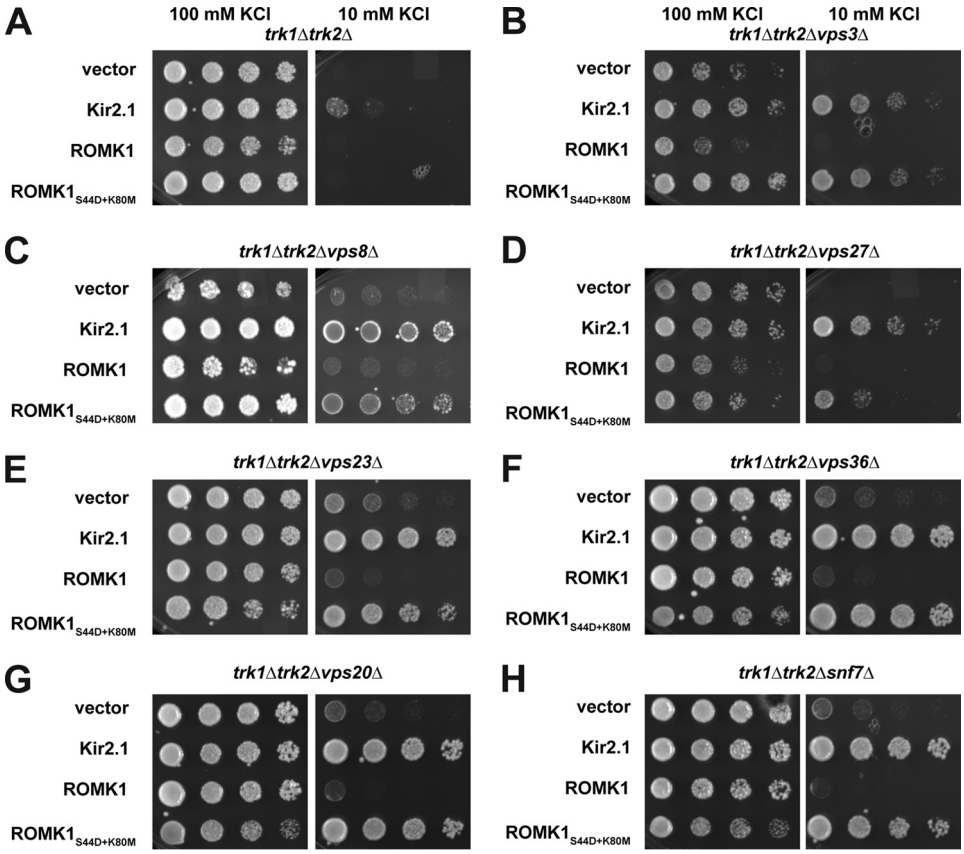

Figure 5. Deletion of genes encoding select ESCRT and CORVET components improves the growth of potassium-sensitive yeast expressing ROMK1$_{S44D+K80M}$. Yeast strains with the indicated genotypes transformed with an empty expression vector control or vectors engineered to express Kir2.1, wildtype ROMK1, or ROMK1$_{S44D+K80M}$ were serially diluted onto medium supplemented with the indicated amounts of KCl. All strains in this figure were identified in the high-throughput SGA screen and then reconstructed *de novo*. All experiments were performed in duplicate, and representative serial dilutions are shown.

yeast and the homologous Nedd4 ligases in mammals (63, 64). Therefore, we hypothesized that disabling Rsp5 would stabilize ROMK1$_{S44D+K80M}$ to a greater degree than ROMK1 because the degradation of ROMK1$_{S44D+K80M}$ was primarily Pep4-dependent (Fig. 2). As anticipated, ROMK1$_{S44D+K80M}$ was completely stable in yeast containing the temperature-sensitive *rsp5-2* allele (Fig. 6*B*). The lack of any Rsp5 dependence on wildtype ROMK1 degradation (Fig. 6*A*) likely reflects the predominant contribution of ERAD to the disposal of this channel (Fig. 3).

How is ROMK activity enhanced in yeast lacking ESCRT, CORVET, or other endosomal sorting genes? Early endosomes are crucial branch points from which cargo may be trafficked in a retrograde fashion to the Golgi apparatus through the action of the Retromer and GARP complexes, sorted into intraluminal vesicles by ESCRT, or recycled directly to the plasma membrane. Direct recycling is known to occur in yeast, although the precise mechanisms are not completely understood (65). We hypothesized that perturbations in ESCRT and other pro-degradation factors shift the dynamic equilibrium of the endosomal population of ROMK toward increased recycling. To test this hypothesis, we crossed our reconstructed *trk1*Δ*trk2*Δ*vps23*Δ strain with *nhx1*Δ yeast, which lack a sodium-proton exchanger involved in endosome acidification and cargo recycling (66). As expected, the *NHX1* deletion ablated ROMK-mediated growth on low-potassium medium in the *trk1*Δ*trk2*Δ*vps23*Δ background (Fig. 6*C*), suggesting that the increase in ROMK activity when ESCRT is perturbed arises from increased recycling.

As the contribution of Nhx1 during cargo recycling is indirect, we sought to replicate this analysis with components of known protein recycling pathways in the cell. We chose Vps5, a BAR domain-containing subunit of the Retromer subcomplex that induces the formation of tubular structures for endosome-to-Golgi recycling (67), and Rcy1, a factor presumed to act upstream of most Vps proteins (68). Surprisingly, deletion of neither *VPS5* (Fig. S6) nor *RCY1* (Fig. S7) in the *trk1*Δ*trk2*Δ*vps23*Δ background ablated ROMK1$_{S44D+K80M}$ activity. These data suggest that ROMK recycling occurs through redundant pathways.

ROMK vacuolar targeting is impeded in yeast deficient in ESCRT components

Having shown that ROMK1$_{S44D+K80M}$ is ERAD-resistant and is regulated by ESCRT and CORVET, we next asked whether ROMK subcellular localization is altered in strains lacking genes encoding select members of these complexes. To this end, we expressed Venus-tagged ROMK$_{K80M}$ (Vn-ROMK) in an ESCRT (*snf7*Δ)- and CORVET (*vps8*Δ)-deficient yeast strain, in the *pep4*Δ mutant, and in an isogenic wild-type strain (*BY4742*). In wildtype yeast, Vn-ROMK partially colocalized with both an mCherry-tagged ER-resident marker, Scs2-mCh

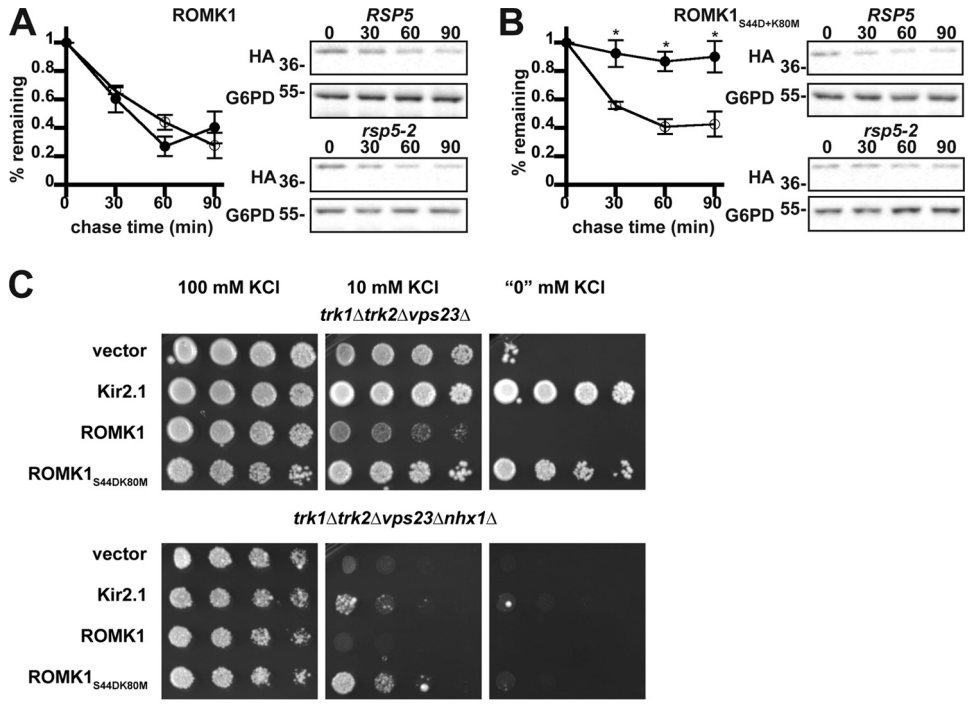

Figure 6. Rsp5 promotes the degradation of ROMK1$_{S44D+K80M}$ and Nhx1 promotes recycling of ROMK. Yeast cultures expressing HA-tagged versions of either ROMK1 (*A*) or ROMK1$_{S44D+K80M}$ (*B*) grown to mid-logarithmic phase were dosed with cycloheximide, and aliquots were withdrawn at 0, 30, 60, and 90 min. Yeast strains containing a temperature-sensitive mutation in the gene encoding Rsp5 (*rsp5-2*, *filled circles*) or wildtype yeast (*RSP5*, *open circles*) expressing ROMK were shifted from room temperature to 39 °C 75 min before addition of cycloheximide. ROMK expression was assessed by Western blotting and normalized to the initial time point. Representative blots are shown, and all blots were stripped and reprobed for glucose-6-phosphate dehydrogenase (*G6PD*) as a loading control. Data represent the means of four independent experiments. *Error bars* show standard errors of the mean, and * indicates a significant ($p < 0.05$) difference as assessed by Student's *t* test. *C*, yeast strains with the indicated genotypes transformed with an empty expression vector control or vectors engineered to express Kir2.1, wildtype ROMK1, or ROMK1S44D+K80M were serially diluted onto medium supplemented with the indicated amounts of KCl. All experiments were performed in duplicate, and a representative assay is shown.

(69), and the dye FM4-64 (70), which binds lipids on the cell surface, passes through the endocytic pathway, and accumulates on the vacuolar limiting membrane (Fig. 7, *A* and *B*). These results are consistent with passage of the protein through the secretory pathway and into a predegradative compartment. In agreement with dual localization, an immunoblot of lysate from wildtype yeast with an antibody that detects GFP derivatives, such as Venus, shows both full-length Vn-ROMK (predicted molecular mass of ~70 kDa) and the free Venus species (predicted molecular mass of ~28 kDa) (Fig. 7*C*). The free Venus species arises from the fact that the fluorescent protein tag is refractory to vacuolar proteolysis (71), so once the Vn-ROMK channel enters a proteolytic compartment the fusion protein is only partially digested. Consistent with this view, Vn-ROMK-derived fluorescence accumulated primarily in the vacuole in *pep4*Δ yeast (Fig. 7, *A* and *B*), and the free Venus species was absent when vacuolar proteases were inactivated (Fig. 7*C*). These data are also consistent with our observation that ROMK1$_{S44D+K80M}$ degradation is primarily vacuolar (Fig. 2*B*).

In the *snf7*Δ ESCRT mutant, Vn-ROMK fluorescence shifts from the ER and vacuole to a large punctum that is adjacent to, but not contiguous with, the vacuolar limiting membrane (Fig. 7, *A* and *B*, see *white arrows*). This localization pattern is consistent with a substrate that is unable to enter intraluminal vesicles and therefore accumulates on the surface of the prevacuolar compartment due to the loss of ESCRT activity in this background (64). Furthermore, the free Venus species is again absent in immunoblot analyses of *snf7*Δ lysates (Fig. 7*C*). Interestingly, a species of ~36 kDa is instead present in this background and not in the isogenic wildtype. The appearance of the band, only in ESCRT mutants, could be due to proteolytic clipping by proteases within the prevacuolar compartment, as its observed molecular weight coincides with a predicted cleavage site between the first and second transmembrane domains of ROMK (data not shown). The fluorescence of Vn-ROMK in other ESCRT mutants (*e.g. vps23*Δ and *vps36*Δ) showed a nearly identical phenotype to *snf7*Δ (data not shown). Finally, to confirm that the Vn-ROMK-enriched puncta in *snf7*Δ cells represents the prevacuolar compartment, we expressed Vn-ROMK in a strain expressing an mCherry-tagged version of the Snf7 protein and found that Vn-ROMK and Snf7-RFP colocalize (Fig. 7*D*, *white arrows*). It was previously observed that the RFP tag interferes with Snf7 function (72), causing a dominant-negative phenotype similar to the genetic null (Fig. 7*C*, compare *lanes 7* and *10*). Therefore, the expression of Snf7-RFP serves both as a marker of the prevacuolar compartment and as an inhibitor of trafficking beyond this compartment.

We also examined localization and Vn-ROMK processing in the *vps8*Δ CORVET mutant. In this strain, Vn-ROMK is primarily present in the ER with little to no vacuolar signal (Fig. 7, *A* and *B*). Furthermore, although the free Venus species accumulates in this background, its levels are reduced relative to the isogenic wildtype strain (Fig. 7*C*). In some *vps8*Δ cells, we observed Vn-ROMK accumulating in small puncta near the outer margin of the cell (Fig. 7*B*, *white arrows*). These results are in accordance with reduced vacuolar delivery in the

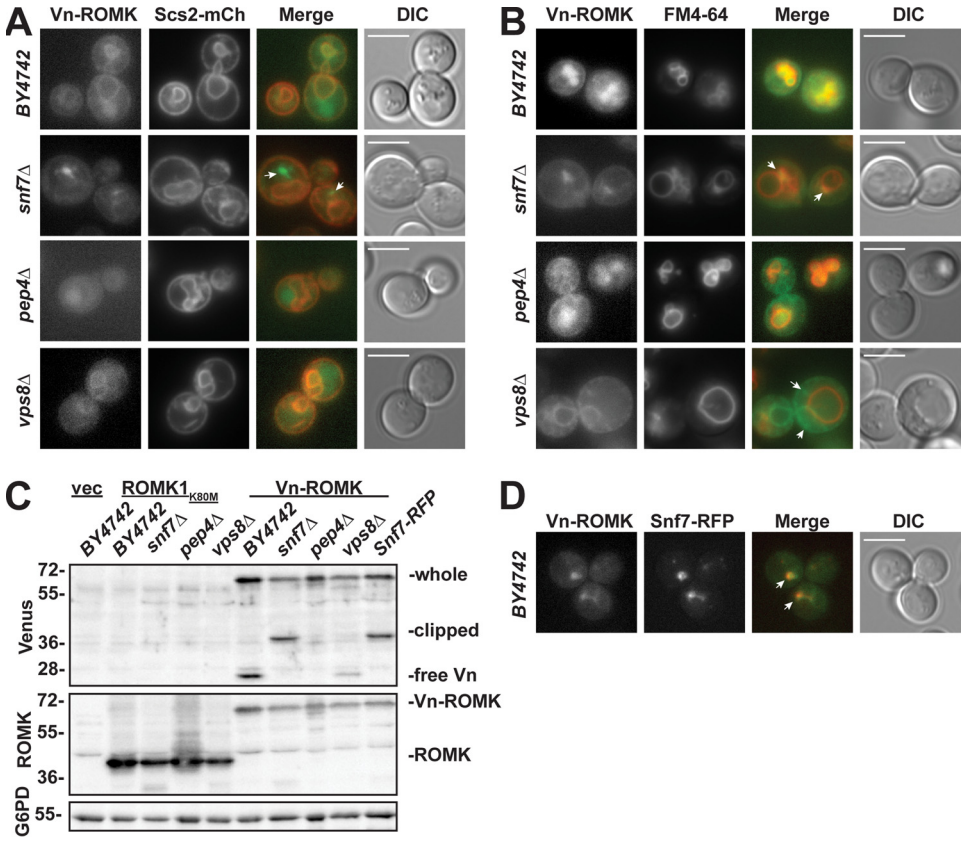

Figure 7. Venus-tagged ROMK$_{K80M}$ (Vn-ROMK) vacuolar trafficking is arrested in ESCRT-deficient yeast and reduced in CORVET-deficient yeast. *A,* epifluorescence live cell images of the indicated yeast strains coexpressing Venus-ROMK$_{K80M}$ (*Vn-ROMK*) and the ER-resident protein Scs2-mCherry (*Scs2-mCh*). *B,* epifluorescence live cell images of the indicated yeast strains expressing Vn-ROMK are shown and were treated with the styryl dye FM4-64 for at least 30 min prior to imaging to stain the endosomal and vacuolar membranes. *C,* Western blot analysis of lysates from yeast of the indicated genetic backgrounds expressing Vn-ROMK or untagged ROMK1$_{K80M}$ or containing an empty expression vector (*vec*) was performed using the indicated antibodies. The Venus epitope migrates as three bands: full-length Vn-ROMK (*whole*), a partially degraded species (*clipped*), and free Venus (*free-Vn*). The blot was stripped and reprobed with an antibody against the ROMK C terminus to show the relative expression of untagged ROMK1$_{K80M}$ (ROMK) and Vn-ROMK. All unlabeled bands are due to non-specific antibody binding (compare with *1st lane "vec"*). Glucose-6-phosphate dehydrogenase (*G6PD*) is also shown as a loading control. *D,* epifluorescence live cell images of yeast coexpressing Vn-ROMK and Snf7-RFP. For all images, a direct interference contrast (*DIC*) image is shown at *right*. The *white scale bar* measures 5 μm. *White arrows* indicate features of interest as described in the text.

*vps8*Δ strain and are in line with localization patterns observed for native yeast substrates in this genetic background (73).

ESCRT and CORVET deplete ROMK from the plasma membrane in HEK293 cells

Given that components in the trafficking and degradation machineries in the late secretory pathway are conserved between yeast and humans, we next asked whether depleting the levels of select components that function in this pathway increases the steady-state distribution of ROMK at the plasma membrane in human cells. To answer this question, we reduced the levels of HGS (the Vps27 homolog), TSG101 (the Vps23 homolog), and VPS8 (the Vps8 homolog) in HEK293 cells that stably express wildtype ROMK1 under the control of an inducible promoter. Next, ROMK at the plasma membrane was biotinylated, captured on beads, and quantified via Western blotting with anti-ROMK antibodies. Robust suppression of TSG101, HGS, and VPS8 protein levels was achieved by siRNA-mediated knockdowns. Moreover, silencing each of these components increased the steady-state levels of ROMK1 at the plasma membrane (Fig. 8*A*). We noted that both immature and mature glycosylated ROMK were biotinylated, as reported previously (74), and that is likely a consequence of ROMK overexpression in these cells. As controls for this experiment, we found that the Na^+/K^+-ATPase α-subunit, ATP1A, was also biotinylated, but its cell-surface expression was unchanged upon knockdown of the ESCRT or CORVET subunits (Fig. 8*A*). In turn, the abundant cytosolic protein, Hsp90, was not biotinylated. Similar results were obtained when this experiment was repeated with a second set of siRNA oligonucleotides (data not shown).

To examine whether ROMK1 was primarily degraded in the lysosome in HEK293 cells, we then performed a cycloheximide chase analysis in the presence or absence of the lysosomal protease inhibitor, leupeptin. As shown in Fig. 8*B*, the addition of leupeptin reduced the rate of ROMK1 degradation relative to the vehicle control. However, treatment with the proteasome inhibitor MG132 had no observable effect on ROMK stability (Fig. 8*B*), indicating that ERAD played a minimal role in degrading ROMK1 in HEK293 cells. These effects were observed for both the mature and immature ROMK species (data not shown). It is important to emphasize that wildtype ROMK1 was used in these experiments because the ROMK1$_{S44D+K80M}$

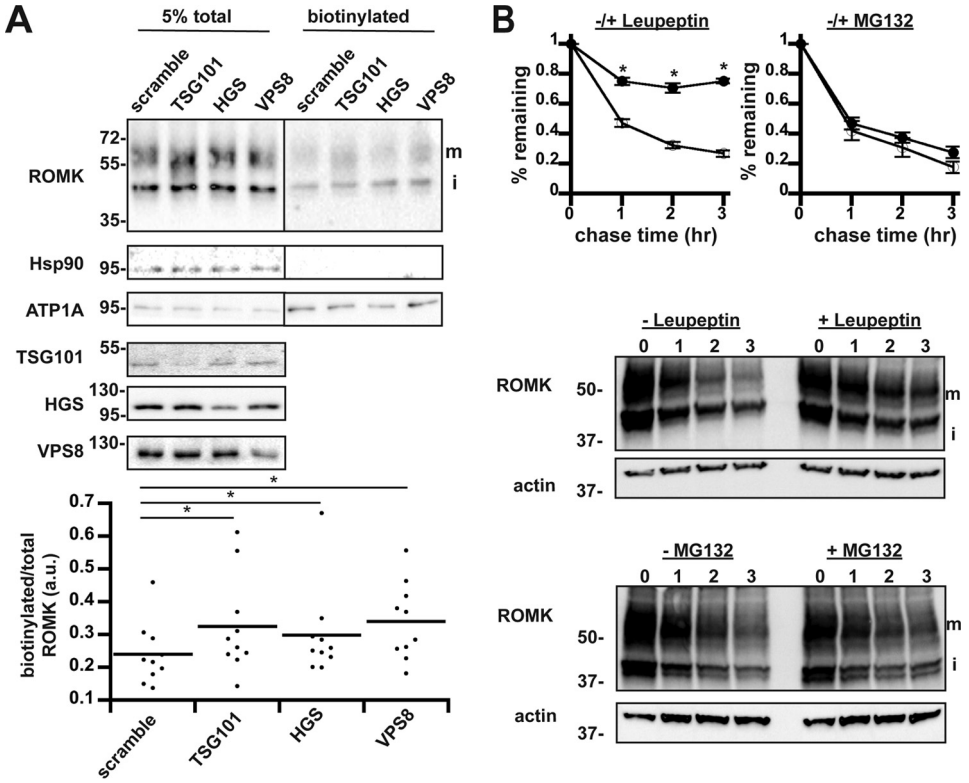

Figure 8. Depletion of select ESCRT and CORVET components increases ROMK surface expression in HEK293 cells. *A,* lysates from HEK293 cells expressing ROMK under the control of the doxycycline-inducible "T-REx" promoter were examined by anti-ROMK immunoblot *in toto* (*left*) or were surface biotinylated and precipitated with NeutrAvidin beads (*right*). ROMK migrates as two bands: an immature (*i*) ER-glycosylated band at ~45 kDa and a larger mature (*m*) glycosylated species of ~55–65 kDa (75). All blots were stripped and reprobed for cytosolic Hsp90 and plasma membrane-enriched ATP1A to show accurate loading and selective biotinylation of only cell-surface proteins. An empty lane between the total and biotinylated samples was cropped out as indicated by the *line*. Quantitation of change in cell-surface ROMK normalized to total protein for each replicate is shown below. Cell lysates from all siRNA-targeted factors were blotted on separate membranes to show efficient knockdown. Silencing for nine experimental replicates led to a decrease of 63 ± 4.7% for TSG101, 71 ± 4.3% for HGS, and 55 ± 5.1% for VPS8. *, $p < 0.05$ (Student's *t* test). *B,* HEK293 cells expressing ROMK under the control of the doxycycline-inducible "T-REx" promoter were pretreated with the lysosomal protease inhibitor leupeptin or MG132 (*closed circles*) or vehicle (*open circles*) for 1 h prior to cycloheximide addition. Samples were harvested at the indicated times. ROMK expression was assessed by Western blotting and normalized to the initial time point. For this figure, only the upper mature band (*m*) was quantitated. Representative blots are shown, and all blots were stripped and reprobed for actin as a loading control. Data represent the means of three independent experiments. *Error bars* show standard errors of the mean, and * indicates a significant ($p < 0.05$) difference as assessed by Student's *t* test.

derivative was only needed in yeast to overcome defects in its trafficking/regulation (also see under "Discussion," below). Nevertheless, these data indicate that ROMK1 degradation in mammalian cells is primarily lysosomal and also utilizes the ESCRT and CORVET complexes to deplete ROMK from the cell surface. Thus, the yeast-based expression system identified evolutionarily conserved trafficking components that influence the biogenesis of human potassium channels in human kidney cells.

Discussion

Surface expression of the ROMK channel in the distal nephron is physiologically down-regulated in states of dietary potassium deprivation by clathrin-dependent endocytosis to safeguard against deleterious potassium loss and to maintain potassium homeostasis (36, 75). Our studies identify components of the trafficking machinery that may underlie a highly regulated pathway that determines whether internalized channels recycle to the surface or are targeted for degradation in the lysosome. Indeed, our genetic screen in yeast revealed that trafficking components involved in endosomal sorting and trafficking act as negative regulators of ROMK. Particularly noteworthy, ROMK regulators included the CORVET subunits Vps3 and Vps8 and the ESCRT subunits Vps27, Vps23, Vps36, Vps20, and Snf7. Knockdown of the human homologs of Vps23, Vps27, and Vps8 increased the density of ROMK at the plasma membrane of HEK293 cells, indicating that negative regulators identified in the yeast screen are also relevant in human cells (Fig. 8).

To explain how inhibition of ESCRT and CORVET genetic components increases ROMK plasma membrane residency, we propose the following model (Fig. 9). Deletion or silencing of ESCRT, CORVET, and other endosomal sorting factors shifts the equilibrium of cargo sorting at early endosomes to favor increased recycling of ROMK to the plasma membrane. Evidence for this model is provided by the abrogation of ROMK function in a yeast strain lacking both an ESCRT component and a recycling component (Fig. 6*C*). It is likely that deletion or silencing of different components produces the same phenotype through different mechanisms, as divergent recycling pathways originate from distinct endosomal populations (65, 76). Indeed, the subcellular localization of Venus-tagged ROMK differs dramatically between yeast strains lacking ESCRT and CORVET components (Fig. 7), despite similar

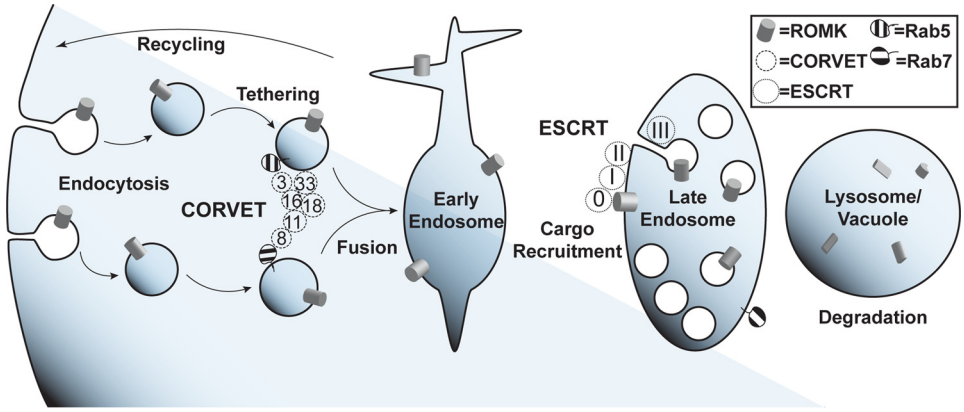

Figure 9. Model of proposed roles for ESCRT and CORVET in ROMK post-endocytic regulation. After endocytosis, ROMK (*gray cylinders*) accumulates in early endosomes. The hexameric CORVET complex (*dotted circles,* "Vps" gene numbers indicated) tethers post-endocytic Rab5-positive vesicles to promote their fusion and maturation into early endosomes. ESCRT proteins (*dashed circles,* complexes 0, I, II, and III) recognize ubiquitinated ROMK and sequester the channel into intraluminal vesicles in late endosomes/multivesicular bodies. These late endosomes eventually mature and fuse with lysosomes in mammalian cells or vacuoles in yeast, where ROMK is degraded.

ROMK function in these strains (Fig. 5). With the exception of the *end3*Δ strain, increased ROMK activity is unlikely due to non-specific inhibition of endocytosis, as deletion of ESCRT and CORVET components does not perturb the rate of endocytosis (73, 77).

The initial screen of the yeast knockout collection uncovered hits in diverse biological pathways, such as endosomal trafficking, mitochondrial function, and translational regulation. As endosomal trafficking is an important determinant of a protein's plasma membrane residency, we chose to focus on trafficking factors. Notably, at least one member each of the four ESCRT complexes, ESCRT-0, ESCRT-I, ESCRT-II, and ESCRT-III, was identified as a hit in the initial screen and confirmed by *de novo* strain construction. The first three ESCRTs act sequentially to identify ubiquitinated cargo for recruitment to inwardly-budding membrane invaginations, whereas ESCRT-III acts as the primary membrane-deforming complex that drives intraluminal vesicle formation (63). The ESCRT-0 subunit Vps27 binds ubiquitinated cargo, as does the ESCRT-I subunit Vps23 (62). The ubiquitin-binding subunit of ESCRT-II, Vps36, was also identified in our screen but as a weaker hit. Because these ubiquitin-binding subunits are themselves ubiquitinated, ESCRT is able to recognize both mono- and polyubiquitinated cargoes (64). Most ESCRT substrates in yeast are ubiquitinated by the Nedd4 homolog Rsp5 (71, 78), which we also found contributes to ROMK1$_{S44D+K80M}$ degradation (Fig. 6*B*) in accordance with the well-characterized role of Nedd4 in regulating ROMK in the kidney in response to fluctuations in dietary potassium (75, 79). Another E3 ligase that acts in the late secretory pathway in yeast, Pib1, can complement Rsp5 activity for some substrates (80–82). Further study is needed to determine how these respective ligases affect ROMK1 ubiquitination and degradation in the yeast system.

CORVET is a hexameric Rab5-positive vesicle-tethering complex consisting of six distinct subunits. Four of these subunits, Vps11, Vps16, Vps18, and Vps33, are also components of the HOPS complex found on Rab7-positive vesicles (56). Recent structural studies have shown that these tethering complexes adopt a disordered and highly flexible conformation that coalesces into a tightly ordered structure upon Rab GTPase binding (83–85). Both of the Rab5-binding subunits that are unique to CORVET, Vps8 and Vps3, were identified in this study as negative regulators of ROMK plasma membrane residence in yeast. Consistent with these data, Vps8 knockdown in mammalian cells increased cell-surface expression of ROMK (Fig. 7). Strikingly, neither the CORVET/HOPS-shared subunits nor the HOPS Rab7-binding subunits were identified as hits in our screen. One model for these data is that CORVET acts upstream of a critical and as yet uncharacterized sorting step for ROMK (Fig. 8). It is also possible that blocking HOPS-mediated tethering arrests ROMK trafficking after it has been packaged into intraluminal vesicles by ESCRT and Vps4, at which point its degradative fate is sealed. Trivially, HOPS function may simply be more tolerant of the loss of individual subunits than CORVET. In addition to binding Rab5, Vps8 also contains a RING E3 ubiquitin ligase domain, which is necessary for tethering (86). However, no specific clients for Vps8 ubiquitination have been found. Therefore, Vps8 ubiquitination may be redundant with other E3 ligases acting at endosomes, notably Rsp5 and Pib1 (see above), yet the CORVET-interacting early endosomal SNARE, Pep12, was also identified as a negative regulator of ROMK. These results lead us to hypothesize that CORVET negatively regulates ROMK by promoting endosome maturation and fusion with lysosomes. To our knowledge, our work represents the first study to genetically link CORVET to the regulation of a specific, clinically relevant cargo, as most mechanistic studies of CORVET have utilized synthetic substrates (87).

Other trafficking-related genes identified as negative regulators of ROMK include the Golgi-localized SNARE *GOS1* and the Retromer encoding factors *VPS5* and *VPS35*. The genes were also identified as negative regulators of Kir2.1 (27). Retromer is a membrane remodeling complex that facilitates cargo retrieval from endosomes either to the plasma membrane or the *trans*-Golgi network and is generally conceived of as being a "pro-recycling" component, thereby acting in opposition to ESCRT-mediated MVB sorting (67). Based on this activity, it is difficult to envision how Retromer functions as a negative regulator of ROMK. However, it is possible that Retromer promotes futile cycling between endosomes and the Golgi, and that

a sub-population of ROMK is freed and recycled to the plasma membrane through alternative pathways in Retromer mutants. In fact, select cargo have been found in multiple model systems to be enriched at the plasma membrane upon Retromer inhibition (88–90).

ROMK may follow a similar trafficking itinerary to that described for the Jen1 lactate permease (91). In this paper, the authors demonstrated that endocytosed Jen1 traffics from endosomes back to the Golgi in a Retromer-dependent fashion before transiting back to the endosome and entering the MVB pathway. In this way, Retromer ultimately stimulates protein degradation by promoting the MVB-vacuolar trafficking of cargo proteins. If ROMK follows a similar route, then internalized ROMK would migrate from endosomes back to the Golgi in a Retromer-dependent fashion, but only as a prequel to ROMK trafficking to the MVB-vacuole for degradation.

The results from this study expand upon our previous work with another inward-rectifying potassium channel, Kir2.1 (27). Surface expression of both channels was suppressed by many of the same components, identifying the late secretory pathway as a key inhibitory trafficking step for inward-rectifying potassium channels. ROMK and Kir2.1 share 42% sequence identity, although neither protein has predicted homology with any endogenous yeast protein (data not shown). Therefore, the yeast trafficking and post-ER degradation machineries may largely be unable to distinguish between the two channels. Nevertheless, we observed some subtle differences. In particular, we found that Kir2.1 increased growth rescue better than ROMK1 in all examined cases. We speculate that this is most likely due to stronger inward rectification of Kir2.1 (92, 93), allowing more potassium influx for growth. In contrast, the fact that select genes identified in this study were absent in the prior screen with Kir2.1 may have resulted from a higher signal to noise ratio due to differences in conductance properties between ROMK and Kir2.1 at the yeast plasma membrane.

The genetic screen described in this report required the use of a non-physiological variant of ROMK1, ROMK1$_{S44D+K80M}$, which contains the phosphomimetic S44D mutation to override an ER-localization signal (94), as well as the K80M mutation to allow ROMK to access its open conformation in the acidic yeast cytosol (47, 52). Our recent work indicates that the K80M mutation is more important than the S44D mutation in promoting ROMK-mediated rescue on low-potassium medium when expressed in the *trk1*Δ*trk2*Δ strain (50). Although we were initially unable to detect a plasma membrane population of ROMK1$_{S44D+K80M}$ by either sucrose density gradient fractionation (Fig. 1*D*) or epifluorescence microscopy (data not shown), a minor fraction of plasma membrane ROMK1$_{S44D+K80M}$ was found in *end3*Δ yeast in which endocytosis is impaired (Fig. S5). Furthermore, rescue of growth on low-potassium media correlates directly with increased intracellular potassium (Fig. 1*C*). This result indicates that ROMK1$_{S44D+K80M}$-mediated growth rescue is due to increased potassium influx. Together, it is likely that yeast require only small amounts of ROMK1$_{S44D+K80M}$ at the plasma membrane to achieve sufficient potassium influx to both increase intracellular potassium and allow for growth on low-potassium media. These data are consistent with the reported high P_o for ROMK (92).

An unforeseen but advantageous consequence of the K80M mutation was that the channel was more ERAD-resistant than wildtype ROMK1 in yeast (Fig. 3). The Lys-80 side chain is predicted by homology modeling to face the intrasubunit interface of the two transmembrane α-helices and acts as a pH-sensitive gate (52). Consequently, the K80M mutation is thought to destabilize the closed state of the channel (52). It is possible that wildtype ROMK1 residing in the low pH cytosol in yeast is in a closed state that is prone to misfolding, which targets the protein for ERAD. In contrast, the ROMK1$_{S44D+K80M}$ derivative is more stable in this environment. Indeed, we recently reported that ROMK1$_{S44D+K80M}$ is less susceptible to *in vitro* proteolysis than wildtype ROMK1 and that trafficking-incompetent mutations in ROMK associated with type II Bartter syndrome destabilize the channel and restore ERAD targeting of ROMK1$_{S44D+K80M}$ (50). It is also noteworthy that neither wildtype ROMK1 nor ROMK1$_{S44D+K80M}$ could rescue growth of potassium-sensitive yeast lacking the ER-resident E3 ubiquitin ligase Doa10 (Fig. S8), indicating that inhibiting ERAD is insufficient to promote the forward trafficking of ROMK in yeast.

The properties of ROMK1$_{S44D+K80M}$ in yeast are analogous to those of wildtype ROMK1 in mammalian cells, as both are primarily substrates for vacuolar/lysosomal degradation (compare Figs. 2*B* and 8*B*). Future studies of ROMK in budding yeast should at minimum include the K80M mutation to ensure that the results will be translatable into mammalian systems.

In conclusion, we have identified key machinery involved in post-endocytic quality control of ROMK. Our findings build upon related work on the inwardly-rectifying potassium channel Kir2.1 (27), the calcium-gated potassium channel KCa3.1 (96), and the voltage-gated potassium channel hERG (97, 98), adding ROMK to a growing list of channels and transporters regulated by post-endocytic transport (99). Previous studies of ROMK in yeast focused instead on the identification of ROMK-interaction partners from human cDNA libraries via the yeast two-hybrid (100, 101). Our report represents the first attempt to use a genome-wide screen for negative regulators of ROMK. In the future, the yeast system could be modified to find positive regulators of ROMK by overexpressing rather than by deleting genes as well as gain-of-function mutations in the channel that alter trafficking or ion permeation.

Experimental procedures

Yeast strain construction, growth conditions, and plasmid construction

A complete list of the strains used in this study is provided in Table S2. All strains were grown at 30 °C unless indicated otherwise. Temperature-sensitive strains were propagated at room temperature prior to temperature shift. Standard procedures were followed for propagation and transformation of yeast (102). Importantly, SC medium used in this study contained 1 g/liter monosodium glutamate instead of ammonium sulfate as

the primary nitrogen source and was buffered with MES to a pH of ~4.5 (27). For serial dilution growth assays, 200-μl cultures were grown overnight with agitation in 96-well dishes in selective liquid medium supplemented with 100 mM KCl and covered with a Breathe-Easy polyurethane membrane (Sigma) to prevent evaporation. Once all cultures reached stationary phase, they were serially diluted 1:5 five times to fill a grid in a standard 96-well plate. Droplets from each dilution were then transferred to SC-Leu solid medium supplemented with 100, 25, 10, and 0 mM KCl using a 48-pin manifold (Sigma). These plates were incubated for 4 days and imaged on days 2–4 using a Bio-Rad Image Station. Medium to which no potassium was added ("0 mM") has been estimated to contain 7–10 mM potassium (42).

Rat ROMK1 was tagged with an HA epitope in the extracellular loop as reported previously (51), and the S44D and K80M mutations were introduced as described recently (50). The manually curated *trk1*Δ*trk2*Δ*xxx*Δ strains originating from this study were made using standard mating, sporulation, and tetrad dissection techniques (102). The genotypes of all parental strains originating from the Yeast Knockout Collection were confirmed by colony PCR prior to mating with YAK01 using the primers indicated in Table S3.

The Venus-ROMK$_{K80M}$ expression vector was made by subcloning the gene encoding ROMK2 into the mVenusC1 (103) expression vector with the restriction enzymes KpnI and AccI. PCR amplification and site-directed mutagenesis were then used to make the Lys → Met mutation analogous to K80M in ROMK1 and to flank Vn-ROMK with XmaI and XhoI restriction sites. These enzymes were then used to subclone Vn-ROMK into the yeast expression vector pRS415.

Synthetic genetic array screening conditions

All screening procedures and media recipes were adapted from protocols published by the Boone laboratory (104), utilized the *trk1*Δ*trk2*Δ strain, and contained a plasmid designed for ROMK1$_{S44D+K80M}$ expression (see above). All yeast manipulations utilized a metal 96-pin manifold (V&P Scientific, San Diego) except for the final transfer onto permissive and selective medium, which used a disposable plastic 96-pin manifold. Briefly, the query strain (YAK01) transformed with the ROMK1$_{S44D+K80M}$ expression vector was mated with the MAT**a** deletion collection (Invitrogen) on YPD plates grown overnight at room temperature. Diploids were selected with SC-Leu containing 200 μg/liter G418 (Research Products International, Mount Prospect, IL), 100 μg/liter clonNAT (Werner BioAgents, Jena, Germany), and 100 mM KCl to maintain potassium sensitivity and hinder the appearance of suppressor mutations. These plates were incubated for 2 days. The diploids were then sporulated onto nitrogen-deficient medium for 5 days at room temperature, and the tetrads were transferred onto SC medium lacking leucine, arginine, histidine, and uracil but containing 200 μg/liter G418, 100 μg/liter clonNAT, and 50 μg/liter L-canavanine (Sigma) to select for desired spores and against unsporulated diploids and undesired spores. Cells on this selective medium were incubated for 2 days, and this step was repeated two times but with 1-day incubations. Finally, the array of triple mutant haploid MAT**a** cells lacking *TRK1, TRK2*, and one other unique non-essential gene were transferred to SC-Leu supplemented with 100 mM KCl and SC-Leu with no additional KCl ("0 mM" potassium). Growth on these plates was assessed by imaging them after 12, 24, and 36 h using the white light setting on a Bio-Rad image station. Rescreening of hits was performed as described above, but with the additional step of transferring the array of triple mutant haploids into 100 μl of liquid SC-Leu medium supplemented with 100 mM KCl in a 96-well dish after the third selection step. These cultures were grown to saturation overnight, and then droplets of liquid culture were transferred onto 0 and 100 mM KCl SC-Leu solid medium with the 96-pin manifold.

Cycloheximide chase analyses

Yeast cultures transformed with human potassium channels expressed under the control of *TEF1* were grown overnight to saturation, diluted into 5 ml of SC-Leu at an A_{600} of 0.25, and grown to mid-log phase, which we define as an A_{600} of 0.7–1.3. Cultures were treated with 150 μg/ml cycloheximide (Sigma) and incubated with agitation in a 37 °C waterbath unless otherwise specified. A total of 1-ml aliquots of culture were withdrawn at the indicated times and immediately harvested and flash-frozen in liquid nitrogen. Aliquots were processed and analyzed for Western blot analysis as described below. For cycloheximide chase analyses of the temperature-sensitive *cdc48-2* strain, all cultures were incubated at 39 °C for 120 min prior to cycloheximide addition. For cycloheximide chase analyses of the temperature-sensitive *ssa1-45* and *rsp5-2* strains, all cultures were incubated at 37 °C for 60 min or 39 °C for 75 min, respectively, prior to cycloheximide addition.

Cycloheximide chase studies in HEK cells were performed 20–24 h after induction with doxycycline. Cells were pretreated with either 10 μM leupeptin (Sigma), 5 μM MG-132 (EMD Millipore, Billerica, MA), or vehicle for 1 h before the addition of cycloheximide (50 μg/ml), and then cells were chased in the presence or absence of the protein degradation inhibitors for 1–3 h. Cell lysates, collected every hour after addition of cycloheximide, were resolved by SDS-PAGE and probed in Western blots with ROMK antibodies (R79 serum (105)).

Analysis of ROMK residence

To perform a sucrose gradient analysis of ROMK residence, yeast cultures transformed with plasmids encoding the indicated channels were grown overnight to saturation, diluted into 200 ml of SC-Leu to an initial A_{600} of 0.25, and then allowed to grow to mid-log phase. A total of 150 A_{600} of cells were harvested and lysed with glass beads in a solution containing 10% sucrose, 10 mM Tris, pH 7.6, 1 mM DTT, 1 mM PMSF (Sigma), 1 μg/ml leupeptin (Sigma), 0.5 μg/ml pepstatin A (Sigma), and 10 mM EDTA (106). The entire volume of the clarified lysate was then layered on top of a sucrose gradient with 1.5 ml of 30% sucrose, 1.5 ml of 40% sucrose, 2.5 ml of 50% sucrose, 1.5 ml of 60% sucrose, 1.5 ml of 65% sucrose, and 2.5 ml of 70% sucrose in the same buffer. The gradients were centrifuged in a Beckman L8–70M ultracentrifuge (Beckman-Coulter, Pasadena, CA) at 28,500 × *g* for 18.5 h. The gradient was then divided into 24 fractions, which were analyzed by SDS-PAGE and Western blotting (see below).

Prior to epifluorescence microscopy, all strains were grown to mid-log phase in SC-Leu media or in SC-Leu-His for strains cotransformed with Scs2-mCh. Cells were placed on a 35-mm poly-D-lysine-coated dish (MatTek, Ashland, MA) and imaged with a Nikon (Tokyo) Eclipse Ti inverted microscope equipped with epifluorescence, an Apo100× objective (NA 1.45), and an Orca Flash 4.0 cMOS (Hamamatsu, Bridgewater, NJ) camera. NIS-Elements software (Nikon) was used to control the imaging parameters, and all images within an experiment were captured used identical acquisition settings. Post-acquisition processing was conducted using ImageJ (National Institutes of Health). To stain the vacuolar membrane, cells were incubated with 300 μM of the FM4-64 dye (Thermo Fisher Scientific) for at least 30 min, which allows for FM4-64 bound to lipid at the cell surface to traffic to the vacuolar-limiting membrane (70), and were washed prior to imaging. All images were acquired at room temperature.

Inductively coupled plasma-mass spectrometry

Yeast cultures transformed with a vector control or a vector engineered for the expression of distinct human potassium channels were grown overnight to saturation, diluted into 7 ml of SC-Leu medium containing either 100 or 10 mM KCl at an A_{600} of 0.2, and allowed to grow for 8 h. Approximately 3.0 A_{600} of cells were harvested by vacuum filtration onto 1.2-μm pore glass fiber membrane filters (EMD Millipore). Next, the cells were washed with 1 μM EDTA and with double-distilled water before they were dissolved in 30% trace metal grade HNO_3 (Fisher) at 65 °C overnight. Solutions were clarified by centrifugation at 20,000 × *g* for 10 min to remove any solid debris and diluted with 2% sub-boil distilled HNO_3 prior to analysis on a PerkinElmer Life Sciences (Waltham, MA) NexION 300× ICP-MS. All elemental concentrations were determined using a 5-point calibration curve. An internal standard of beryllium, germanium, and thallium was added to all samples to assess signal strength and instrument drift. A 2% nitric acid blank was run every seven samples to assess signal memory effects. All biological replicates were run in technical duplicates, and the technical replicates are the average of three replicate measurements from the ICP-MS.

HEK293 cell culture and siRNA knockdown

All cells were propagated at 37 °C in a 5% CO_2-humidified incubator, and all cells were passaged every 3–4 days using standard methods. All experiments were conducted after seven or fewer passages. T-REx-HEK293 ROMK cells were a generous gift from the laboratory of Dr. J. Denton (74), and the original T-REx-HEK293 cells were purchased from Invitrogen. Upon receipt, they were tested for mycoplasma using a PCR-based kit (ATCC, Manassas, VA) and found to be negative. T-REx-HEK293 ROMK cells were propagated in high-glucose for Dulbecco's modified Eagle's medium (Sigma) supplemented with 10% fetal bovine serum, 5 μg/ml blasticidin S, and 250 μg/ml hygromycin B to maintain selection for the integrated tetracycline-inducible ROMK cassette (48). To induce ROMK expression, cells were treated with 2 μg/ml tetracycline for at least 24 h. siRNA silencing was achieved with 1.5 μg/ml Lipofectamine RNAiMax (Thermo Fisher Scientific) transfection reagent and 10 nM RNA duplex (GE Healthcare) (sequences are indicated in Table S3). Lipofectamine and RNA were incubated separately in 0.25 ml of prewarmed OptiMEM (Thermo Fisher Scientific) for 5 min, mixed at a 1:1 volumetric ratio, incubated for another 5 min, and then added to cells. After 24 h, culture media were changed, and the transfection protocol was repeated a second time.

HEK293 cell-surface biotinylation

Prior to biotinylation, cells at 80–90% confluency were treated with 125 μg/ml cycloheximide for 2 h to increase the cell-surface concentration of ROMK. The cells were washed three times with Dulbecco's phosphate-buffered saline (DPBS) and then treated with 0.3 mg/ml EZ-Link Sulfo-NHS Biotin (Thermo Fisher Scientific) for 1 h. Excess biotin was quenched by washing the cells with 100 mM glycine in DPBS three times; the cells were lysed in HEENG buffer (20 mM HEPES, pH 7.6, 1 mM EDTA, 1 mM EGTA, 25 mM NaCl, 10% glycerol) containing 1% Triton X-100 and cOmplete, Mini, EDTA-free protease inhibitors (Roche Diagnostics, Mannheim, Germany) for 1 h, and the mixture was centrifuged for 5 min at maximum speed to remove any insoluble material. Soluble protein concentrations were assessed with a Pierce BCA protein assay kit (Thermo Fisher Scientific) per the manufacturer's instructions. For each condition, 300 μg of protein was added to 30 μl of Pierce NeutrAvidin-agarose (Thermo Fisher Scientific) beads, brought to a total volume of 1 ml, and incubated overnight. Beads were then triple washed with DPBS and treated with 1× SDS-PAGE sample buffer for 1 h at room temperature prior to SDS-PAGE and Western blot analysis (see below). All steps of this protocol were conducted at 4 °C.

Western blot analysis

To assay protein expression in yeast, equivalent A_{600} cultures at mid-log growth phase were lysed in 300 mM NaOH, 1 mM 2-mercaptoethanol, 1 mM PMSF (Sigma), 1 μg/ml leupeptin (Sigma), and 0.5 μg/ml pepstatin A (Sigma). Total protein was precipitated from lysate with 5% trichloroacetic acid (TCA), resuspended in SDS-PAGE sample buffer, incubated for at least 1 h at room temperature, and analyzed by SDS-PAGE (95). Steady-state levels of protein in HEK293 cells were analyzed by dissolving 30 μg of protein from clarified lysate in SDS-PAGE sample buffer, incubation for at least 1 h, and SDS-PAGE.

All Western blots were developed with the SuperSignal West enhanced chemiluminescence kit (Thermo Fisher Scientific) per the manufacturer's instructions. Chemiluminescence images were obtained on a Bio-Rad image station. Quantitation of signal intensity was performed by measuring integrated pixel density in ImageJ (National Institutes of Health). Relevant antibody information is supplied in Table S4.

Author contributions—J. L. B., A. R. S., A. F. O., and P. A. W. conceived and guided the study. T. D. M. designed, performed, and analyzed all experiments expect for those described in Fig. 8*B*, which were designed and performed by B. K. A. F. O. provided equipment and guidance for epifluorescence microscopy and D. J. B. provided equipment and guidance for ICP-MS. T. D. M. drafted the document, which was edited and approved for publication by all authors.

Acknowledgments—We thank Dr. Jerod Denton (Vanderbilt University) for providing the HEK293 T-REx ROMK cell line and for useful discussions and advice. The Scs2-mCherry plasmid was provided by the laboratory of Dr. Susan Michaelis (Johns Hopkins University), and the Snf7-RFP strain was provided by the laboratory of Dr. Martha Cyert (Stanford University). Dr. Robert Piper (University of Iowa), Dr. Christian Ungermann (Universität Osnabrück), and Dr. Jason MacGurn (Vanderbilt University) provided useful discussion and advice. Assorted strains, reagents, and equipment were kindly provided by the research groups of Dr. Karen Arndt (University of Pittsburgh), Dr. Manoj Puthenveedu (Carnegie Mellon University), Dr. Ora Weisz (University of Pittsburgh), Dr. Elizabeth Miller (Colombia University), Dr. Antony Cooper (University of New South Wales), and Dr. Linda Hicke (University of Texas). Technical assistance was provided by Dr. Brighid O'Donnell, Jackson Parr, and Yang Liu.

Note added in proof—The version of this paper that was published as a Paper in Press on January 8, 2018 inadvertently omitted Table S4. The supporting table has been uploaded.

References

1. Balchin, D., Hayer-Hartl, M., and Hartl, F. U. (2016) *In vivo* aspects of protein folding and quality control. *Science* **353,** aac4354
2. Ellgaard, L., McCaul, N., Chatsisvili, A., and Braakman, I. (2016) Co- and post-translational protein folding in the ER. *Traffic* **17,** 615–638 CrossRef Medline
3. Preston, G. M., and Brodsky, J. L. (2017) The evolving role of ubiquitin modification in endoplasmic reticulum-associated degradation. *Biochem. J.* **474,** 445–469 CrossRef Medline
4. Gottschling, D. E., and Nyström, T. (2017) The upsides and downsides of organelle interconnectivity. *Cell* **169,** 24–34 CrossRef Medline
5. Schmidt, M., and Finley, D. (2014) Regulation of proteasome activity in health and disease. *Biochim. Biophys. Acta* **1843,** 13–25 CrossRef Medline
6. Geva, Y., and Schuldiner, M. (2014) The back and forth of cargo exit from the endoplasmic reticulum. *Curr. Biol.* **24,** R130–R136 CrossRef Medline
7. Arvan, P., Zhao, X., Ramos-Castaneda, J., and Chang, A. (2002) Secretory pathway quality control operating in Golgi, plasmalemmal, and endosomal systems. *Traffic* **3,** 771–780 CrossRef Medline
8. MacGurn, J. A. (2014) Garbage on, garbage off: new insights into plasma membrane protein quality control. *Curr. Opin. Cell Biol.* **29,** 92–98 CrossRef Medline
9. Gajewski, C., Dagcan, A., Roux, B., and Deutsch, C. (2011) Biogenesis of the pore architecture of a voltage-gated potassium channel. *Proc. Natl. Acad. Sci. U.S.A.* **108,** 3240–3245 CrossRef Medline
10. Lukacs, G. L., and Verkman, A. S. (2012) CFTR: folding, misfolding and correcting the ΔF508 conformational defect. *Trends Mol. Med.* **18,** 81–91 CrossRef Medline
11. Young, J. C. (2014) The role of the cytosolic HSP70 chaperone system in diseases caused by misfolding and aberrant trafficking of ion channels. *Dis. Model. Mech.* **7,** 319–329 CrossRef Medline
12. Lukacs, G. L., Mohamed, A., Kartner, N., Chang, X. B., Riordan, J. R., and Grinstein, S. (1994) Conformational maturation of CFTR but not its mutant counterpart (ΔF508) occurs in the endoplasmic reticulum and requires ATP. *EMBO J.* **13,** 6076–6086 Medline
13. Ward, C. L., and Kopito, R. R. (1994) Intracellular turnover of cystic fibrosis transmembrane conductance regulator. Inefficient processing and rapid degradation of wildtype and mutant proteins. *J. Biol. Chem.* **269,** 25710–25718 Medline
14. Rabeh, W. M., Bossard, F., Xu, H., Okiyoneda, T., Bagdany, M., Mulvihill, C. M., Du, K., di Bernardo, S., Liu, Y., Konermann, L., Roldan, A., and Lukacs, G. L. (2012) Correction of both NBD1 energetics and domain interface is required to restore ΔF508 CFTR folding and function. *Cell* **148,** 150–163 CrossRef Medline
15. Mendoza, J. L., Schmidt, A., Li, Q., Nuvaga, E., Barrett, T., Bridges, R. J., Feranchak, A. P., Brautigam, C. A., and Thomas, P. J. (2012) Requirements for efficient correction of ΔF508 CFTR revealed by analyses of evolved sequences. *Cell* **148,** 164–174 CrossRef Medline
16. Sharma, M., Pampinella, F., Nemes, C., Benharouga, M., So, J., Du, K., Bache, K. G., Papsin, B., Zerangue, N., Stenmark, H., and Lukacs, G. L. (2004) Misfolding diverts CFTR from recycling to degradation. *J. Cell Biol.* **164,** 923–933 CrossRef Medline
17. Luciani, A., Villella, V. R., Esposito, S., Brunetti-Pierri, N., Medina, D., Settembre, C., Gavina, M., Pulze, L., Giardino, I., Pettoello-Mantovani, M., D'Apolito, M., Guido, S., Masliah, E., Spencer, B., Quaratino, S., *et al.* (2010) Defective CFTR induces aggresome formation and lung inflammation in cystic fibrosis through ROS-mediated autophagy inhibition. *Nat. Cell Biol.* **12,** 863–875 CrossRef Medline
18. Li, K., Jiang, Q., Bai, X., Yang, Y.-F., Ruan, M.-Y., and Cai, S.-Q. (2016) Tetrameric assembly of K^+ channels requires ER-located chaperone proteins. *Mol. Cell* **65,** 1–14
19. Gong, Q., Keeney, D. R., Molinari, M., and Zhou, Z. (2005) Degradation of trafficking-defective long QT syndrome type II mutant channels by the ubiquitin-proteasome pathway. *J. Biol. Chem.* **280,** 19419–19425 CrossRef Medline
20. Anderson, C. L., Delisle, B. P., Anson, B. D., Kilby, J. A., Will, M. L., Tester, D. J., Gong, Q., Zhou, Z., Ackerman, M. J., and January, C. T. (2006) Most LQT2 Mutations reduce Kv11.1 (hERG) current by a class 2 (trafficking-deficient) mechanism. *Circulation* **113,** 365–373 CrossRef Medline
21. Wang, Y., Huang, X., Zhou, J., Yang, X., Li, D., Mao, H., Sun, H. H., Liu, N., and Lian, J. (2012) Trafficking-deficient G572R-hERG and E637K-hERG activate stress and clearance pathways in endoplasmic reticulum. *PLoS ONE* **7,** e29885 CrossRef Medline
22. Buck, T. M., Plavchak, L., Roy, A., Donnelly, B. F., Kashlan, O. B., Kleyman, T. R., Subramanya, A. R., and Brodsky, J. L. (2013) The Lhs1/GRP170 chaperones facilitate the endoplasmic reticulum-associated degradation of the epithelial sodium channel. *J. Biol. Chem.* **288,** 18366–18380 CrossRef Medline
23. Gao, Y., Bertuccio, C. A., Balut, C. M., Watkins, S. C., and Devor, D. C. (2012) Dynamin- and Rab5-dependent endocytosis of a Ca^{2+}-activated K^+ channel, KCa2.3. *PLoS ONE* **7,** e44150 CrossRef Medline
24. Donnelly, B. F., Needham, P. G., Snyder, A. C., Roy, A., Khadem, S., Brodsky, J. L., and Subramanya, A. R. (2013) Hsp70 and Hsp90 multichaperone complexes sequentially regulate thiazide-sensitive cotransporter endoplasmic reticulum-associated degradation and biogenesis. *J. Biol. Chem.* **288,** 13124–13135 CrossRef Medline
25. Gao, Y., Yechikov, S., Vazquez, A. E., Chen, D., and Nie, L. (2013) Distinct roles of molecular chaperones HSP90α and HSP90β in the biogenesis of KCNQ4 channels. *PLoS ONE* **8,** e57282 CrossRef Medline
26. Iwai, C., Li, P., Kurata, Y., Hoshikawa, Y., Morikawa, K., Maharani, N., Higaki, K., Sasano, T., Notsu, T., Ishido, Y., Miake, J., Yamamoto, Y., Shirayoshi, Y., Ninomiya, H., Nakai, A., *et al.* (2013) Hsp90 prevents interaction between CHIP and HERG proteins to facilitate maturation of wildtype and mutant HERG proteins. *Cardiovasc. Res.* **100,** 520–528 CrossRef Medline
27. Kolb, A. R., Needham, P. G., Rothenberg, C., Guerriero, C. J., Welling, P. A., and Brodsky, J. L. (2014) ESCRT regulates surface expression of the Kir2.1 potassium channel. *Mol. Biol. Cell* **25,** 276–289 CrossRef Medline
28. Seaayfan, E., Defontaine, N., Demaretz, S., Zaarour, N., and Laghmani, K. (2016) OS9 interacts with NKCC2 and targets its immature form for the endoplasmic-reticulum-associated degradation pathway. *J. Biol. Chem.* **291,** 4487–4502 CrossRef Medline
29. Hirota, Y., Kurata, Y., Kato, M., Notsu, T., Koshida, S., Inoue, T., Kawata, Y., Miake, J., Bahrudin, U., Li, P., Hoshikawa, Y., Yamamoto, Y., Igawa, O., Shirayoshi, Y., Nakai, A., *et al.* (2008) Functional stabilization of Kv1.5 protein by Hsp70 in mammalian cell lines. *Biochem. Biophys. Res. Commun.* **372,** 469–474 CrossRef Medline
30. Zhou, H., Tate, S. S., and Palmer, L. G. (1994) Primary structure and functional properties of an epithelial K channel. *Am. J. Physiol.* **266,** C809–C824 CrossRef Medline
31. Wang, W. H., Schwab, A., and Giebisch, G. (1990) Regulation of small-conductance K^+ channel in apical membrane of rat cortical collecting tubule. *Am. J. Physiol.* **259,** F494–F502 Medline

32. Frindt, G., Shah, A., Edvinsson, J., and Palmer, L. G. (2009) Dietary K regulates ROMK channels in connecting tubule and cortical collecting duct of rat kidney. *Am. J. Physiol. Renal Physiol.* **296,** F347–F354 CrossRef Medline
33. Ho, K., Nichols, C. G., Lederer, W. J., Lytton, J., Vassilev, P. M., Kanazirska, M. V., and Hebert, S. C. (1993) Cloning and expression of an inwardly rectifying ATP-regulated potassium channel. *Nature* **362,** 31–38 CrossRef Medline
34. Leung, Y.-M., Zeng, W. Z., Liou, H. H., Solaro, C. R., and Huang, C. L. (2000) Phosphatidylinositol 4,5-bisphosphate and intracellular pH regulate the ROMK1 potassium channel via separate but interrelated mechanisms. *J. Biol. Chem.* **275,** 10182–10189 CrossRef Medline
35. Welling, P. A., and Ho, K. (2009) A comprehensive guide to the ROMK potassium channel: form and function in health and disease. *Am. J. Physiol. Renal Physiol.* **297,** F849–F863 CrossRef Medline
36. Zeng, W.-Z., Babich, V., Ortega, B., Quigley, R., White, S. J., Welling, P. A., and Huang, C.-L. (2002) Evidence for endocytosis of ROMK potassium channel via clathrin-coated vesicles. *Am. J. Physiol. Renal Physiol.* **283,** F630–F639 CrossRef Medline
37. Lin, D.-H., Yue, P., Pan, C.-Y., Sun, P., Zhang, X., Han, Z., Roos, M., Caplan, M., Giebisch, G., and Wang, W.-H. (2009) POSH stimulates the ubiquitination and the clathrin-independent endocytosis of ROMK1 channels. *J. Biol. Chem.* **284,** 29614–29624 CrossRef Medline
38. Fang, L., Garuti, R., Kim, B.-Y., Wade, J. B., and Welling, P. A. (2009) The ARH adaptor protein regulates endocytosis of the ROMK potassium secretory channel in mouse kidney. *J. Clin. Invest.* **119,** 3278–3289 Medline
39. Simon, D. B., Karet, F. E., Rodriguez-Soriano, J., Hamdan, J. H., DiPietro, A., Trachtman, H., Sanjad, S. A., and Lifton, R. P. (1996) Genetic heterogeneity of Bartter's syndrome revealed by mutations in the K^+ channel, ROMK. *Nat. Genet.* **14,** 152–156 CrossRef Medline
40. Ji, W., Foo, J. N., O'Roak, B. J., Zhao, H., Larson, M. G., Simon, D. B., Newton-Cheh, C., State, M. W., Levy, D., and Lifton, R. P. (2008) Rare independent mutations in renal salt handling genes contribute to blood pressure variation. *Nat. Genet.* **40,** 592–599 CrossRef Medline
41. Peters, M., Ermert, S., Jeck, N., Derst, C., Pechmann, U., Weber, S., Schlingmann, K. P., Seyberth, H. W., Waldegger, S., and Konrad, M. (2003) Classification and rescue of ROMK mutations underlying hyperprostaglandin E syndrome/antenatal Bartter syndrome. *Kidney Int.* **64,** 923–932 CrossRef Medline
42. Nakamura, R. L., and Gaber, R. F. (1998) Studying ion channels using yeast genetics. *Methods Enzymol. Methods Enzymol.* **293,** 89–104 CrossRef Medline
43. Bichet, D., Lin, Y.-F., Ibarra, C. A., Huang, C. S., Yi, B. A., Jan, Y. N., and Jan, L. Y. (2004) Evolving potassium channels by means of yeast selection reveals structural elements important for selectivity. *Proc. Natl. Acad. Sci. U.S.A.* **101,** 4441–4446 CrossRef Medline
44. Haass, F. A., Jonikas, M., Walter, P., Weissman, J. S., Jan, Y.-N., Jan, L. Y., and Schuldiner, M. (2007) Identification of yeast proteins necessary for cell-surface function of a potassium channel. *Proc. Natl. Acad. Sci. U.S.A.* **104,** 18079–18084 CrossRef Medline
45. Minor, D. L., Jr., Masseling, S. J., Jan, Y. N., and Jan, L. Y. (1999) Transmembrane structure of an inwardly rectifying potassium channel. *Cell* **96,** 879–891 CrossRef Medline
46. Grishin, A., Li, H., Levitan, E. S., and Zaks-Makhina, E. (2006) Identification of γ-aminobutyric acid receptor-interacting factor 1 (TRAK2) as a trafficking factor for the K^+ channel Kir2.1. *J. Biol. Chem.* **281,** 30104–30111 CrossRef Medline
47. Paynter, J. J., Shang, L., Bollepalli, M. K., Baukrowitz, T., and Tucker, S. J. (2010) Random mutagenesis screening indicates the absence of a separate H^+-sensor in the pH-sensitive Kir channels. *Channels* **4,** 390–397 CrossRef Medline
48. Raphemot, R., Weaver, C. D., and Denton, J. S. (2013) High-throughput screening for small-molecule modulators of inward rectifier potassium channels. *J. Vis. Exp.* **2013,** 4209 Medline
49. Giaever, G., Chu, A. M., Ni, L., Connelly, C., Riles, L., Véronneau, S., Dow, S., Lucau-Danila, A., Anderson, K., André, B., Arkin, A. P., Astromoff, A., El-Bakkoury, M., Bangham, R., Benito, R., *et al.* (2002) Functional profiling of the *Saccharomyces cerevisiae* genome. *Nature* **418,** 387–391 CrossRef Medline
50. O'Donnell, B. M., Mackie, T. D., Subramanya, A. R., and Brodsky, J. L. (2017) Endoplasmic reticulum-associated degradation of the renal potassium channel, ROMK, leads to type II Bartter syndrome. *J. Biol. Chem.* **292,** 12813–12827 CrossRef Medline
51. Yoo, D., Kim, B. Y., Campo, C., Nance, L., King, A., Maouyo, D., and Welling, P. A. (2003) Cell surface expression of the ROMK (Kir 1.1) channel is regulated by the aldosterone-induced kinase, SGK-1, and protein kinase A. *J. Biol. Chem.* **278,** 23066–23075 CrossRef Medline
52. Rapedius, M., Fowler, P. W., Shang, L., Sansom, M. S., Tucker, S. J., and Baukrowitz, T. (2007) H bonding at the helix-bundle crossing controls gating in Kir potassium channels. *Neuron* **55,** 602–614 CrossRef Medline
53. Barreto, L., Canadell, D., Petrezsélyová, S., Navarrete, C., Maresová, L., Peréz-Valle, J., Herrera, R., Olier, I., Giraldo, J., Sychrová, H., Yenush, L., Ramos, J., and Ariño, J. (2011) A genomewide screen for tolerance to cationic drugs reveals genes important for potassium homeostasis in *Saccharomyces cerevisiae*. *Eukaryot. Cell* **10,** 1241–1250 CrossRef Medline
54. MacGurn, J. A., Hsu, P.-C., and Emr, S. D. (2012) Ubiquitin and membrane protein turnover: from cradle to grave. *Annu. Rev. Biochem.* **81,** 231–259 CrossRef Medline
55. Woolford, C. A., Daniels, L. B., Park, F. J., Jones, E. W., Van Arsdell, J. N., and Innis, M. A. (1986) The PEP4 gene encodes an aspartyl protease implicated in the posttranslational regulation of *Saccharomyces cerevisiae* vacuolar hydrolases. *Mol. Cell. Biol.* **6,** 2500–2510 CrossRef Medline
56. Balderhaar, H. J., Lachmann, J., Yavavli, E., Bröcker, C., Lürick, A., and Ungermann, C. (2013) The CORVET complex promotes tethering and fusion of Rab5/Vps21-positive membranes. *Proc. Natl. Acad. Sci. U.S.A.* **110,** 3823–3828 CrossRef Medline
57. Kingsbury, J. M., Sen, N. D., Maeda, T., Heitman, J., and Cardenas, M. E. (2014) Endolysosomal membrane trafficking complexes drive nutrient-dependent TORC1 signaling to control cell growth in *Saccharomyces cerevisiae*. *Genetics* **196,** 1077–1089 CrossRef Medline
58. Plemel, R. L., Lobingier, B. T., Brett, C. L., Angers, C. G., Nickerson, D. P., Paulsel, A., Sprague, D., and Merz, A. J. (2011) Subunit organization and Rab interactions of Vps-C protein complexes that control endolysosomal membrane traffic. *Mol. Biol. Cell* **22,** 1353–1363 CrossRef Medline
59. Lachmann, J., Glaubke, E., Moore, P. S., and Ungermann, C. (2014) The Vps39-like TRAP1 is an effector of Rab5 and likely the missing Vps3 subunit of human CORVET. *Cell Logist.* **4,** e970840 CrossRef Medline
60. Perini, E. D., Schaefer, R., Stöter, M., Kalaidzidis, Y., and Zerial, M. (2014) Mammalian CORVET is required for fusion and conversion of distinct early endosome subpopulations. *Traffic* **15,** 1366–1389 CrossRef Medline
61. Pols, M. S., ten Brink, C., Gosavi, P., Oorschot, V., and Klumperman, J. (2013) The HOPS proteins hVps41 and hVps39 are required for homotypic and heterotypic late endosome fusion. *Traffic* **14,** 219–232 CrossRef Medline
62. Babst, M. (2005) A protein's final ESCRT. *Traffic* **6,** 2–9 CrossRef Medline
63. Henne, W. M., Stenmark, H., and Emr, S. D. (2013) Molecular mechanisms of the membrane sculpting ESCRT pathway. *Cold Spring Harb. Perspect. Biol.* **5,** a016766 CrossRef Medline
64. Stringer, D. K., and Piper, R. C. (2011) A single ubiquitin is sufficient for cargo protein entry into MVBs in the absence of ESCRT ubiquitination. *J. Cell Biol.* **192,** 229–242 CrossRef Medline
65. MacDonald, C., and Piper, R. C. (2016) Cell surface recycling in yeast: mechanisms and machineries. *Biochem. Soc. Trans.* **44,** 474–478 CrossRef Medline
66. Kojima, A., Toshima, J. Y., Kanno, C., Kawata, C., and Toshima, J. (2012) Localization and functional requirement of yeast Na^+/H^+ exchanger, Nhx1p, in the endocytic and protein recycling pathway. *Biochim. Biophys. Acta* **1823,** 534–543 CrossRef Medline
67. Burd, C., and Cullen, P. J. (2014) Retromer: a master conductor of endosome sorting. *Cold Spring Harb. Perspect. Biol.* **6,** a016774 CrossRef Medline
68. Wiederkehr, A., Avaro, S., Prescianotto-Baschong, C., Haguenauer-Tsapis, R., and Riezman, H. (2000) The F-box protein Rcy1p is involved in endocytic membrane traffic and recycling out of an early endosome in *Saccharomyces cerevisiae*. *J. Cell Biol.* **149,** 397–410 CrossRef Medline

69. Zhou, C., Slaughter, B. D., Unruh, J. R., Guo, F., Yu, Z., Mickey, K., Narkar, A., Ross, R. T., McClain, M., and Li, R. (2014) Organelle-based aggregation and retention of damaged proteins in asymmetrically dividing cells. *Cell* **159,** 530–542 CrossRef Medline
70. Vida, T. A., and Emr, S. D. (1995) A new vital stain for visualizing vacuolar membrane dynamics and endocytosis in yeast. *J. Cell Biol.* **128,** 779–792 CrossRef Medline
71. Guiney, E. L., Klecker, T., and Emr, S. D. (2016) Identification of the endocytic sorting signal recognized by the Art1-Rsp5 ubiquitin ligase complex. *Mol. Biol. Cell* **27,** 4043–4054 CrossRef Medline
72. Huh, W.-K., Falvo, J. V., Gerke, L. C., Carroll, A. S., Howson, R. W., Weissman, J. S., and O'Shea, E. K. (2003) Global analysis of protein localization in budding yeast. *Nature* **425,** 686–691 CrossRef Medline
73. Luo, Wj., and Chang, A. (2000) An endosome-to-plasma membrane pathway involved in trafficking of a mutant plasma membrane ATPase in yeast. *Mol. Biol. Cell* **11,** 579–592 CrossRef Medline
74. Fallen, K., Banerjee, S., Sheehan, J., Addison, D., Lewis, L. M., Meiler, J., and Denton, J. S. (2009) The Kir channel immunoglobulin domain is essential for Kir1.1 (ROMK) thermodynamic stability, trafficking and gating. *Channels* **3,** 57–68 CrossRef Medline
75. Al-Qusairi, L., Basquin, D., Roy, A., Rajaram, R. D., Maillard, M. P., Subramanya, A. R., and Staub, O. (2017) Renal tubular ubiquitin-protein ligase NEDD4-2 is required for renal adaptation during long-term potassium depletion. *J. Am. Soc. Nephrol.* **28,** 2431–2442 CrossRef Medline
76. van Weering, J. R., and Cullen, P. J. (2014) Membrane-associated cargo recycling by tubule-based endosomal sorting. *Semin. Cell Dev. Biol.* **31,** 40–47 CrossRef Medline
77. Wiederkehr, A., Meier, K. D., and Riezman, H. (2001) Identification and characterization of *Saccharomyces cerevisiae* mutants defective in fluid-phase endocytosis. *Yeast* **18,** 759–773 CrossRef Medline
78. Erpapazoglou, Z., Dhaoui, M., Pantazopoulou, M., Giordano, F., Mari, M., Léon, S., Raposo, G., Reggiori, F., and Haguenauer-Tsapis, R. (2012) A dual role for K63-linked ubiquitin chains in multivesicular body biogenesis and cargo sorting. *Mol. Biol. Cell* **23,** 2170–2183 CrossRef Medline
79. Ronzaud, C., Loffing-Cueni, D., Hausel, P., Debonneville, A., Malsure, S. R., Fowler-Jaeger, N., Boase, N. A., Perrier, R., Maillard, M., Yang, B., Stokes, J. B., Koesters, R., Kumar, S., Hummler, E., Loffing, J., and Staub, O. (2013) Renal tubular NEDD4–2 deficiency causes NCC-mediated salt-dependent hypertension. *J. Clin. Invest.* **123,** 657–665 Medline
80. Shin, M. E., Ogburn, K. D., Varban, O. A., Gilbert, P. M., and Burd, C. G. (2001) FYVE domain targets Pib1p ubiquitin ligase to endosome and vacuolar membranes. *J. Biol. Chem.* **276,** 41388–41393 CrossRef Medline
81. Nikko, E., and Pelham, H. R. (2009) Arrestin-mediated endocytosis of yeast plasma membrane transporters. *Traffic* **10,** 1856–1867 CrossRef Medline
82. Kampmeyer, C., Karakostova, A., Schenstrøm, S. M., Abildgaard, A. B., Lauridsen, A.-M., Jourdain, I., and Hartmann-Petersen, R. (2017) The exocyst subunit Sec3 is regulated by a protein quality control pathway. *J. Biol. Chem.* **292,** 15240–15253 CrossRef Medline
83. Chou, H.-T., Dukovski, D., Chambers, M. G., Reinisch, K. M., and Walz, T. (2016) CATCHR, HOPS and CORVET tethering complexes share a similar architecture. *Nat. Struct. Mol. Biol.* **23,** 761–763 CrossRef Medline
84. Murray, D. H., Jahnel, M., Lauer, J., Avellaneda, M. J., Brouilly, N., Cezanne, A., Morales-Navarrete, H., Perini, E. D., Ferguson, C., Lupas, A. N., Kalaidzidis, Y., Parton, R. G., Grill, S. W., and Zerial, M. (2016) An endosomal tether undergoes an entropic collapse to bring vesicles together. *Nature* **537,** 107–111 CrossRef Medline
85. Bröcker, C., Kuhlee, A., Gatsogiannis, C., Balderhaar, H. J., Hönscher, C., Engelbrecht-Vandré, S., Ungermann, C., and Raunser, S. (2012) Molecular architecture of the multisubunit homotypic fusion and vacuole protein sorting (HOPS) tethering complex. *Proc. Natl. Acad. Sci. U.S.A.* **109,** 1991–1996 CrossRef Medline
86. Horazdovsky, B. F., Cowles, C. R., Mustol, P., Holmes, M., and Emr, S. D. (1996) A novel RING finger protein, Vps8p, functionally interacts with the small GTPase, Vps21p, to facilitate soluble vacuolar protein localization. *J. Biol. Chem.* **271,** 33607–33615 CrossRef Medline
87. Galmes, R., ten Brink, C., Oorschot, V., Veenendaal, T., Jonker, C., van der Sluijs, P., and Klumperman, J. (2015) Vps33B is required for delivery of endocytosed cargo to lysosomes. *Traffic* **16,** 1288–1305 CrossRef Medline
88. Dang, H., Klokk, T. I., Schaheen, B., McLaughlin, B. M., Thomas, A. J., Durns, T. A., Bitler, B. G., Sandvig, K., and Fares, H. (2011) Derlin-dependent retrograde transport from endosomes to the Golgi apparatus. *Traffic* **12,** 1417–1431 CrossRef Medline
89. Xia, W.-F., Tang, F.-L., Xiong, L., Xiong, S., Jung, J.-U., Lee, D.-H., Li, X.-S., Feng, X., Mei, L., and Xiong, W.-C. (2013) Vps35 loss promotes hyperresorptive osteoclastogenesis and osteoporosis via sustained RANKL signaling. *J. Cell Biol.* **200,** 821–837 CrossRef Medline
90. Choy, R. W., Park, M., Temkin, P., Herring, B. E., Marley, A., Nicoll, R. A., and von Zastrow, M. (2014) Retromer mediates a discrete route of local membrane delivery to dendrites. *Neuron* **82,** 55–62 CrossRef Medline
91. Becuwe, M., and Léon, S. (2014) Integrated control of transporter endocytosis and recycling by the arrestin-related protein Rod1 and the ubiquitin ligase Rsp5. *Elife* 10.7554/eLife.03307
92. Choe, H., Palmer, L. G., and Sackin, H. (1999) Structural determinants of gating in inward-rectifier K^+ channels. *Biophys. J.* **76,** 1988–2003 CrossRef Medline
93. Hibino, H., Inanobe, A., Furutani, K., Murakami, S., Findlay, I., and Kurachi, Y. (2010) Inwardly rectifying potassium channels: their structure, function, and physiological roles. *Physiol. Rev.* **90,** 291–366 CrossRef Medline
94. Yoo, D., Fang, L., Mason, A., Kim, B.-Y., and Welling, P. A. (2005) A phosphorylation-dependent export structure in ROMK (Kir 1.1) channel overrides an endoplasmic reticulum localization signal. *J. Biol. Chem.* **280,** 35281–35289 CrossRef Medline
95. Zhang, Y., Nijbroek, G., Sullivan, M. L., McCracken, A. A., Watkins, S. C., Michaelis, S., and Brodsky, J. L. (2001) Hsp70 molecular chaperone facilitates endoplasmic reticulum-associated protein degradation of cystic fibrosis transmembrane conductance regulator in yeast. *Mol. Biol. Cell* **12,** 1303–1314 CrossRef Medline
96. Balut, C. M., Hamilton, K. L., and Devor, D. C. (2012) Trafficking of intermediate (KCa3.1) and small (KCa2.x) conductance, Ca^{2+}-activated K^+ channels: a novel target for medicinal chemistry efforts? *ChemMedChem* **7,** 1741–1755 CrossRef Medline
97. Guo, J., Massaeli, H., Xu, J., Jia, Z., Wigle, J. T., Mesaeli, N., and Zhang, S. (2009) Extracellular K^+ concentration controls cell surface density of IKr in rabbit hearts and of the HERG channel in human cell lines. *J. Clin. Invest.* **119,** 2745–2757 CrossRef Medline
98. Apaja, P. M., Foo, B., Okiyoneda, T., Valinsky, W. C., Barriere, H., Atanasiu, R., Ficker, E., Lukacs, G. L., and Shrier, A. (2013) Ubiquitination-dependent quality control of hERG K^+ channel with acquired and inherited conformational defect at the plasma membrane. *Mol. Biol. Cell* **24,** 3787–3804 CrossRef Medline
99. Apaja, P. M., and Lukacs, G. L. (2014) Protein homeostasis at the plasma membrane. *Physiology* **29,** 265–277 CrossRef Medline
100. Bundis, F., Neagoe, I., Schwappach, B., and Steinmeyer, K. (2006) Involvement of Golgin-160 in cell surface transport of renal ROMK channel: co-expression of golgin-160 increases ROMK currents. *Cell Physiol. Biochem.* **17,** 1–12 CrossRef Medline
101. Renigunta, A., Mutig, K., Rottermann, K., Schlichthörl, G., Preisig-Müller, R., Daut, J., Waldegger, S., and Renigunta, V. (2011) The glycolytic enzymes glyceraldehyde 3-phosphate dehydrogenase and enolase interact with the renal epithelial K^+ channel ROMK2 and regulate its function. *Cell. Physiol. Biochem.* **28,** 663–672 CrossRef Medline
102. Adams, A., and Kaiser, C. A. (1998) *Methods in Yeast Genetics: A Cold Spring Harbor Laboratory Course Manual*, Cold Spring Harbor Laboratory Press, Plainview, NY
103. Koushik, S. V., Chen, H., Thaler, C., Puhl, H. L., 3rd., and Vogel, S. S. (2006) Cerulean, Venus, and VenusY67C FRET reference standards. *Biophys. J.* **91,** L99–L101 CrossRef Medline
104. Tong, A. H., and Boone, C. (2006) Synthetic genetic array analysis in *Saccharomyces cerevisiae*. *Methods Mol. Biol.* **313,** 171–192 Medline
105. Wade, J. B., Fang, L., Coleman, R. A., Liu, J., Grimm, P. R., Wang, T., and Welling, P. A. (2011) Differential regulation of ROMK (Kir1.1) in distal nephron segments by dietary potassium. *Am. J. Physiol. Renal Physiol.* **300,** F1385–F1393 CrossRef Medline
106. Roberg, K. J., Rowley, N., and Kaiser, C. A. (1997) Physiological regulation of membrane protein sorting late in the secretory pathway of *Saccharomyces cerevisiae*. *J. Cell Biol.* **137,** 1469–1482 CrossRef Medline